Energy 262 (2023) 125496

Contents lists available at ScienceDirect

Energy

journal homepage: www.elsevier.com/locate/energy

Negative carbon dioxide gas power plant integrated with gasification of sewage sludge

Paweł Ziółkowski *, Kamil Stasiak, Milad Amiri, Dariusz Mikielewicz

Gdańsk University of Technology, Faculty of Mechanical Engineering and Ship Technology, Institute of Energy, G. Narutowicza 11/12, 80-233, Gdańsk, Poland

ARTICLE INFO

Keywords:
Bioenergy with carbon capture and storage
Thermodynamic analysis
CO2 negative power plant
Gas-steam turbine bleed
Waste gasification
Energy-from-waste

ABSTRACT

One of the primary objectives of the negative carbon dioxide gas power plant (nCO_2PP) is to develop an innovative technology confirming the possibility of the use of sewage sludge to produce electricity while having a positive impact on the environment. In this paper, a mathematical model is presented to estimate thermodynamic parameters of the system in relation to the gasification process and changes in such parameters in the bleeds as well as temperature and pressure. The main novelty of this paper is the integration of the gas-steam turbine model with the gasification reactor model in such a way that the effect of the gasification products on the turbine output is established. In turn, parameters from the turbine bleed directly affect the gasification process and cause feedback for the system. Developed code allows determination of parameters such as efficiency of the proposed nCO_2PP cycle, gas composition from the gasifier, temperature in the gas turbine bleed and other related information. The synergy between the CCS plant and the proposed utilization of sewage sludge (which is considered as a renewable energy source) enables the installation to achieve negative overall emissions of CO_2.

1. Introduction

Nowadays there are two major problems facing future generations, namely waste disposal and the generation of electricity without emissions [1]. A solution that combines both aspects is the generation of electricity using waste. One of the most problematic residues of everyday human activity is sewage sludge by account of all its smell, going through the problems of decomposition of the substances contained in it, and finally the legal aspects of its management [2]. An important aspect when estimating the necessary power is a proper mathematical model depicting the phenomena occurring in individual devices. Most constituent elements of the thermodynamic cycle are already simulated in a sufficiently accurate way to predict the cycle parameters, as confirmed in the authors' works [3,4]. An additional aspect is the need for acquiring relevant procedures for carbon capture to reduce carbon footprint for future generations. Leading techniques for that purpose include post-combustion, pre-combustion and oxy-combustion [5–7]. Carbon Capture and Storage (CSS) technology is considered an important "bridging technology", allowing effective abatement of CO_2 emissions for power units using fossil fuels [8,9]. However, if biomass is used as a fuel in a power plant equipped with the CCS system, the negative CO_2 emissions can be achieved in the light of the fact that biomass is regarded as a renewable fuel. In practice, wide development of such technologies would enable not only reduction of CO_2 emissions, but also reversal of the harmful effects done so far. In the long term, wide application of technologies with carbon-negative emissions could allow returning to pre-industrial concentrations of CO_2 in the atmosphere [10] and can be helpful for sustainable solutions also in heat generation [11,12].

Thermal gasification is essentially a high-severity pyrolysis in the presence of gasification agent, followed by reduction of gases on a solid phase (carbon) [13]. Gasification agent can be either a single compound, e.g. air, oxygen, carbon dioxide, steam, or a mixture of the aforementioned gases [14]. Gasification can be used for conversion of solid fuel into a combustible mixture of gases, which enables the use of the chemical energy of solid fuels in cycles incorporating gas turbines. Thus, it enables utilization of solid fuels in cycles different than Rankine cycle. An example of a cycle, utilising gasification in combination with gas turbine and Carbon Capture and Storage is shown in Fig. 1. The focus of this paper is on correct modelling the gasification process. Negative CO_2 gas turbine power plant proposal and a detailed description of the negative emission power plant cycle are presented in the authors'

* Corresponding author.
E-mail addresses: pawel.ziolkowski1@pg.edu.pl (P. Ziółkowski), kamil.stasiak@pg.edu.pl (K. Stasiak), milad.amiri@pg.edu.pl (M. Amiri), dariusz.mikielewicz@pg.edu.pl (D. Mikielewicz).

https://doi.org/10.1016/j.energy.2022.125496
Received 29 April 2022; Received in revised form 14 September 2022; Accepted 17 September 2022
Available online 28 September 2022

previous work [4].

However, considerable difficulties are arising in the modelling of gasification issues, namely the use of different gasifying agents [15], or the adaptation of energy and environmental conditions to gas turbine systems [16], including those with microturbines [17].

Determination of applicable methods and parameters for sewage sludge gasification is a prelude to the design of a gasification plant. In principle, there is a classification of individual modelling approaches distinguishing the reliance on thermodynamic equilibrium, modelling of process kinetics, local approach (CFD) and artificial intelligence [18–20].

Integral gasification reactor models using thermodynamic equilibrium are most often based on assumptions such as sufficient bed residence time to reach steady state and neglecting of carbon or tar formation. Nonetheless, these approaches are called stoichiometric models, which are basically further divided into the ones based on 1) determining the equilibrium constants of chemical reactions, or 2) minimizing the Gibbs free energy [14,19,21–28]. The use of the equilibrium approach is related to the idealization of the process. Since non-equilibrium phenomena occur in reality in the reactor, equilibrium estimates deviate from measurements obtained in experiments. Often, to reflect the experiment more accurately, it becomes necessary to include empirical correction factors [14,19,21–24,26–28]. However, the essential advantage of equilibrium models is their fundamental ease in combining with entire thermodynamic cycles so as to indicate the possibility of integrating a power plant with a gasification reactor [29]. Kinetic models, in contrast to equilibrium thermodynamics, are characterized by time dependence and the adoption of characteristic time scales [18,26,30]. Kinetic models are usually multidimensional models which are composed of computational stages, each representing a different section of the gasifying unit, essentially useful for the design of a gasifying system [31,32].

Hundreds of models are described in the literature and a significant number of them is available in commercial codes [33,34]. These are useful for gasifier design, optimization, and retrofit, but still need experimental verification. CFD modelling of coal gasification in entrained flow gasifiers focuses on devolatilization kinetics and gas phase and surface reactions [35]. However, the CFD models are usually coupled structures where the accompanying processes are important, i.e., turbulence influences the reaction rate, and the occurring reactions influence the turbulence intensity. This approach is becoming increasingly useful in the design and subsequent optimization of gasification systems [36]. However, kinetic and CDF approaches are often characterized by the need to create geometries and, above all, require time-consuming calculations, which significantly limits their application in thermal power cycles [37].

There have been studies published that used simulation of the gasification process using Aspen Plus, which generated results with high accuracy compared to available experimental data [38,39]. However, none of the previous simulation studies used sewage sludge that was gasified using exhaust gases from a gas turbine bleed.

It should be mentioned that relatively similar systems, namely gas-steam units also have not been integrated at this level thus far. In such systems the gasification process is supplied with a part of the required heat from the air compressor cooling [31,32], and the remaining part of the heat is steam from the steam turbine bleed [29]. This represents a very interesting solution, but the peculiarity of the resulting gas in the auto-thermal reformer (ATR) is the high nitrogen content and thus the higher energy intensity.

The main objective of this work is to model the integration of gasification process of sewage sludge in a reactor (R) with CO_2 negative power plant (see Fig. 1). Negative CO_2 emission for electricity production is possible using a novel concept based on oxy-combustion in the wet combustion chamber followed by separation of water from CO_2 mixture using a compact spray ejector condenser, followed by compression of separated CO_2. Therefore, the aim of this work is to indicate the basic parameters relating to the gas produced from gasification and the inclusion of this process in the mass and energy balance of the whole cycle. The article aims to determine parameters at key factors of the thermodynamic cycle to estimate performance of a gas power plant with a gas created from the gasification of sewage sludge (SS). Another aim of the article is to indicate the values of negative CO_2 emissions vs bleed pressure.

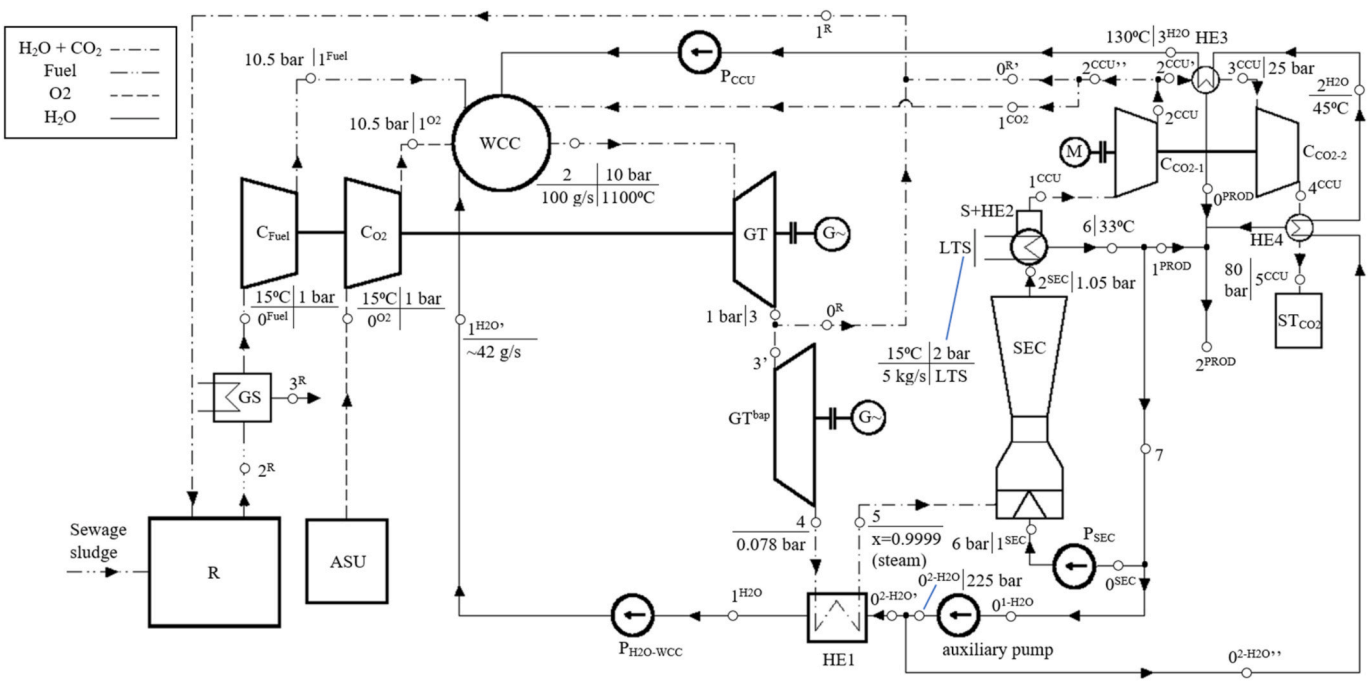

Fig. 1. Negative CO_2 emission gas power plant process flow diagram with sewage sludge gasification.

2. Thermodynamic cycle of nCO2PP integrated with gasification

The integration of gasification process of sewage sludge in a reactor (R) with CO_2 negative power plant is presented in Figs. 1 and 2. When analysing the diagrams, it is important to note that water is marked with a solid line so that it is injected into the two crucial devices of the cycle, namely the Wet Combustion Chamber (WCC) and the Spray-Ejector Condenser (SEC). In WCC, the working fluid (H_2O + CO_2 mixture) is produced which then flows to the stages of the gas-steam turbine. This gas flows through successive stages until it reaches the extraction point marked 3, where it is split into a 0^R flow directed to the reactor and a 3′ flow which enters the other stages of the low-pressure turbine. The bleed pressure was tested in the range 0.7–1.6 bar, but nevertheless the gas turbine in this area can be divided into a high-pressure part (GT) and a low-pressure part (GT^{bap}), where the excellent part of the fluid mixture expands below the ambient pressure. It is worth tracing the path of the exhaust gas taken from the extraction hood (0^R), which then mixes with a small amount of CO_2 from the first carbon dioxide compressor ($0^{R,*}$), and then, reaching uniform parameters at point 1^R, flows into the reactor. It should be added that also a negligible amount of the stream from the first CO_2 compressor (1^{CO2}) enters the combustion chamber, so that a total of five streams is injected into it. The 4 remaining ones are the stream of oxygen from the compressor (C_{O2}), fuel from gasification (C_{Fuel}), water from two different pumps ($P_{H2O\text{-}WCC}$ and P_{CCU}). Most of the other equipment including spray-ejector condenser (SEC), CO_2 capture unit compressors 1 and 2, ($C_{CO2\text{-}1,2}$), Fuel Compressor (C_{fuel}), Oxygen Compressor (C_{O2}), Water Pump supplying supercritical water ($P_{H2O\text{–}WCC}$), Water Pump supplying SEC (P_{SEC}), Separator with Heat Exchanger 2 (S + HE2), Heat Exchanger 1, 3 and 4 (HE1,3,4), Motor (M), Low-temperature source (LTS), CO_2 Storage Tank (ST_{CO2}) are discussed in the paper [4]. The individual nodal points for the cycle under scrutiny are presented in a *T-s* diagram.

In Figs. 1 and 2 a particular attention has been paid to the process occurring in the gasification reactor (R) as well as in the Gas Scrubber (GS). As a result of two processes, namely, 1) mixing of the sewage sludge with the gas stream from the bleed and 2) reactions taking place inside the gasification reactor, the temperature of the whole mixture is raised and gas with parameters corresponding to 2^R is formed. Thus, as can be seen from the *T-s* diagram, the sludge is first heated isobarically, then the moisture contained in it is isobarically and isothermally phase transformed, and then the gasification reaction takes place at a constant pressure but raising the temperature of the resulting mixture above the extraction temperature. It is also important that the gas is purified in the gas scrubber (GS), so there are no components such as H_2O, SO_2 and N_2 at the outlet of this device.

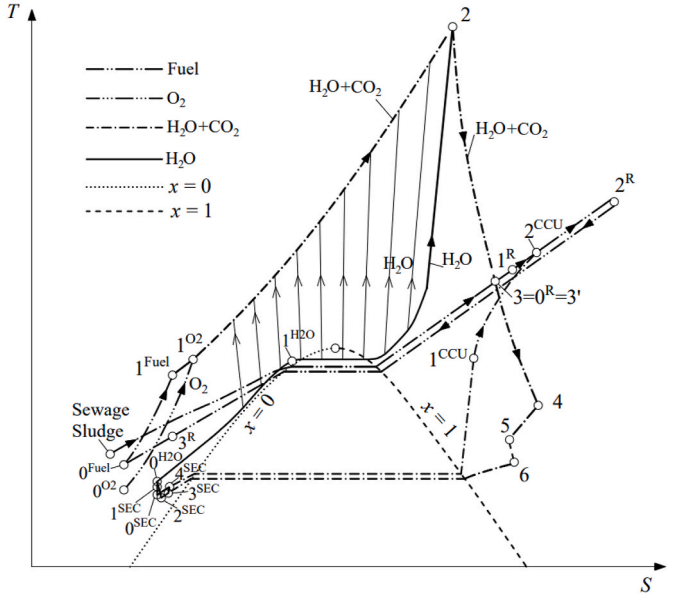

Fig. 2. T-s diagram of negative CO_2 emission gas power plant with sewage sludge gasification.

More information about conventional steam-gas systems, including a proposal for a gas-steam condenser were described in publications [40,41]. In the wet combustion chamber (WCC), the combustion reaction of the near stoichiometric mixture of oxygen and fuel takes place. The WCC is cooled with water, which when becomes steam, mixes with flue gases, creating a high-pressure vapour, reaching a pressure of 40 bar in the first consideration of this system [42]. The working mixture at such pressure and temperature is close to the operational parameters of commonly known gas turbines [42,43].

It is worth to mention about different types of cycles with the use of oxy-combustion, namely:

1. The Water Cycle [44–48], where approximately 90% of the medium is water vapour, and the remaining part is CO_2 resulting from combustion. However, integration with a gasification reactor has not yet been considered in this system.
2. The GRAZ cycle [49–52] is a more complex system, operating largely on steam and allowing to achieve higher efficiency. It, likewise, uses oxy-combustion and introduces different types of fuel, but it was largely targeted at the combustion of hydrogen.
3. Other systems using oxy-combustion, but with the predominance of carbon dioxide in the flow system, are:
   - Semi-Closed Oxy-fuel Combustion Combined Cycle [53];
   - CO_2 Prevented Emissions Recuperative Advanced Turbine Energy [54,55];
   - MATIANT [56–58];
   - CO_2 Loop for Energy and Nature, Enhanced by Refrigeration and Gas-turbines [59];
   - Steam gas turbine engine in multi-fuel and multi-functional energy systems [60].

All the above cycles are not integrated by bleed in the gas turbine, but only focus on achieving the required parameters to capture carbon dioxide. The articles in which there is a bleed of the medium do not use it for the gasification process, but most often the flow of exhaust gas is directed to the backpressure exchangers [52,61].

3. Zero-dimensional mathematical modelling of thermodynamic cycle with gasifier

The robust mathematical models respect mass, momentum and energy balance equations in the integrated form (also called 0D) [52,61–66]. In this section, computational procedures for gasifier and gas scrubber are presented, basing on authors previous publication [3]. The thermodynamic model of the real gas, output power and the efficiencies are also defined.

3.1. Chemical reaction and equilibrium constant

The Boudouard reaction, the water-gas reaction, the formation reaction for methane, the water-gas the shift reaction and the formation reaction for propane in gasification are taken into consideration, respectively:

$$C + CO_{2(g)} \rightleftharpoons 2CO_{(g)} + 172.62 \left[\frac{kJ}{kmol}\right] \quad (1)$$

$$C + H_2O_{(g)} \rightleftharpoons CO_{(g)} + H_{2(g)} + 131.22 \left[\frac{kJ}{kmol}\right] \quad (2)$$

$$C + 2H_{2(g)} \rightleftharpoons CH_{4(g)} - 74.9 \left[\frac{kJ}{kmol}\right] \quad (3)$$

$$CO_{2(g)} + H_{2(g)} \rightleftharpoons CO_{(g)} + H_2O_{(g)} + 41.39 \left[\frac{kJ}{kmol}\right] \quad (4)$$

$$3C + 4H_{2(g)} \rightleftharpoons C_3H_{8(g)} - 34.63 \left[\frac{kJ}{kmol}\right] \quad (5)$$

in which subscript g describes gaseous phase component and the enthalpies of formation for reactions are presented, respectively. The equilibrium constants are determined to quantify the chemical equilibria, where the right side of the following reaction indicating its direction is always in the counter of the equilibrium constant equation. For the equilibrium equation of each reaction, only the gaseous phase component mole fractions are taken into consideration [14,67]:

- Boudouard reaction:

$$K_{(1)} = \frac{x_{CO}^2}{x_{CO_2}} p \quad (6)$$

in which:
p – pressure of the process in [atm],
x_{CO}, x_{CO2} – molar fraction of CO, CO_2 in [%mol].

- Water-gas reaction:

$$K_{(2)} = \frac{x_{CO} \cdot x_{H_2}}{x_{H_2O}} p \quad (7)$$

where:
x_{H_2}, x_{H_2O} – molar fraction of H_2, H_2O in [%mol].

- Formation reaction for methane:

$$K_{(3)} = \frac{x_{CH_4}}{x_{H_2}^2} \cdot \frac{1}{p} \quad (8)$$

in which:
x_{CH_4} – molar fraction of CH_4 in [%mol].

- Water-gas shift reaction:

$$K_{(4)} = \frac{x_{CO} \cdot x_{H_2O}}{x_{CO_2} \cdot x_{H_2}} \quad (9)$$

- Formation reaction for propane:

$$K_{(5)} = \frac{x_{C_3H_8}}{x_{H_2}^4} \cdot \frac{1}{p^3} \quad (10)$$

in which:
$x_{C_3H_8}$ – molar fraction of C_3H_8 in [%mol].

3.2. Robust equilibrium constants estimation

Specific value of the equilibrium constants $K_{(1)}$, $K_{(2)}$, $K_{(3)}$, $K_{(4)}$, $K_{(5)}$ are specified according to different models to calculate these equilibrium constants ranging from very detailed to simplified methods and those that were approximately tailored to resemble the real conditions, which example are in Refs. [14,68]. For the gasification model, the equilibrium constants approximation from $K_{(1)}$, to $K_{(4)}$, have been derived by Gumz [68], however, for propane formation equilibrium constant ($K_{(5)}$) has been specified from Nernst approximate method [14]. Approximations assume that equilibrium constants may be corrected by considering multiplicative factors $k_{K_{(1)}}, \ldots, k_{K_{(5)}}$ to account for the actual distance of a real gasifier from the ideal equilibrium state, as follows [68]:

$$K_{(1)} = k_{K_{(1)}} \cdot 10^{\left(3.26730 - \frac{8820.690}{T} - 1.208714 \cdot 10^{-3} T + 0.153734 \cdot 10^{-6} \cdot T^2 + 2.295483 \cdot lgT\right)} \quad (11)$$

$$K_{(2)} = k_{K_{(2)}} \cdot 10^{\left(0.8255488 \cdot 10^{-6} \cdot T^2 + 14.515670 \cdot lgT - \frac{4825.986}{T} - 5.671122 \cdot 10^{-3} \cdot T - 33.45778\right)} \quad (12)$$

$$K_{(3)} = k_{K_{(3)}} \cdot 10^{\left(\frac{4662.80}{T} - 2.09594 \cdot 10^{-3} T + 0.38620 \cdot 10^{-6} T^2 + 3.034338 \cdot lgT - 13.06361\right)} \quad (13)$$

$$K_{(4)} = k_{K_{(4)}} \cdot 10^{\left(36.72508 - \frac{3994.704}{T} + 4.462408 \cdot 10^{-3} T - 0.671814 \cdot 10^{-6} \cdot T^2 - 12.220277 \cdot lgT\right)} \quad (14)$$

$$K_{(5)} = k_{K_{(5)}} \cdot 10^{\left(-2.96 - 14.143 \cdot lgT + \frac{5427.7}{T}\right)} \quad (15)$$

in which:
T – temperature of the process in [K],
$k_{K_{(1)}}, \ldots, k_{K_{(5)}}$ – tuning coefficients obtained empirically.

3.3. The amount of fuel and converter

In this subsection, the mole number of elements per 1 kmole of feedstock and per 1 kmole of gasifying agent (converter) are defined. Feedstock ingredients such as carbon, hydrogen, oxygen, nitrogen, sulphur, moisture, are, as follows:

$$(C)_{fuel} = \frac{C}{M_C} \cdot M_{fuel} \left[\frac{\text{kmol C}}{\text{kmol fuel}}\right] \quad (16)$$

$$(H)_{fuel} = \left(\frac{H}{M_{H_2O}} + 2 \cdot \frac{w_{fuel}}{M_{H_2O}}\right) \cdot M_{fuel} \left[\frac{\text{kmol H}}{\text{kmol fuel}}\right] \quad (17)$$

$$(O)_{fuel} = \left(\frac{O}{M_O} + \frac{w_{fuel}}{M_{H_2O}}\right) \cdot M_{fuel} \left[\frac{\text{kmol O}}{\text{kmol fuel}}\right] \quad (18)$$

$$(N)_{fuel} = \frac{N}{M_N} \cdot M_{fuel} \left[\frac{\text{kmol N}}{\text{kmol fuel}}\right] \quad (19)$$

$$(S)_{fuel} = \frac{S}{M_S} \cdot M_{fuel} \left[\frac{\text{kmol S}}{\text{kmol fuel}}\right] \quad (20)$$

where:
C, H, O, N, S – mass fractions of elements in the feedstock,
M_{fuel} – molar weight of fuel feedstock in [kg/kmol],
M_C, M_O, M_N, M_{H_2O}, M_S – molar weights of elements and water in the feedstock in [kg/kmol],
w_{fuel} – moisture mass fraction in the feedstock.

The converter ingredients such as air, steam, carbon dioxide, and moisture are included in the following relationships to calculate elements mole concentration [14,68]:

$$(C)_{con} = \frac{\gamma_{CO_2}}{1 + \beta_{steam} + \gamma_{CO_2}} \left[\frac{\text{kmol C}}{\text{kmol con.}}\right] \quad (21)$$

$$\text{or } (C)_{con} = x_{CO_2}^{con} \left[\frac{\text{kmol C}}{\text{kmol con.}}\right] \quad (22)$$

$$(H)_{con} = \frac{2 \cdot \left(\beta_{steam} + \frac{0.79 \cdot M_{N_2} + 0.21 \cdot M_{O_2}}{M_{H_2O}} X_{air}\right)}{1 + \beta_{steam} + \gamma_{CO_2}} \left[\frac{\text{kmol H}}{\text{kmol con.}}\right] \quad (23)$$

$$\text{or} \quad (H)_{con} = 2 \cdot x_{H_2O}^{con} \left[\frac{\text{kmol H}}{\text{kmol con.}}\right] \tag{24}$$

$$(O)_{con} = \frac{2 \cdot \left(\left(1 - \frac{0.79 \cdot M_{N_2} + 0.21 \cdot M_{O_2}}{M_{H_2O}} X_{air} \right) \cdot 0.21 + \gamma_{CO_2} \right) + \beta_{steam}}{1 + \beta_{steam} + \gamma_{CO_2}} \left[\frac{\text{kmol O}}{\text{kmol con.}}\right] \tag{25}$$

$$\text{or} \quad (O)_{con} = 2 \cdot \left(x_{O_2}^{con} + x_{CO_2}^{con} \right) + x_{H_2O}^{con} \left[\frac{\text{kmol O}}{\text{kmol con.}}\right] \tag{26}$$

$$(N)_{con} = \frac{2 \cdot \left(1 - \frac{0.79 \cdot M_{N_2} + 0.21 \cdot M_{O_2}}{M_{H_2O}} X_{air} \right) \cdot (1 - 0.21)}{1 + \beta_{steam} + \gamma_{CO_2}} \left[\frac{\text{kmol N}}{\text{kmol con.}}\right] \tag{27}$$

$$\text{or} \quad (N)_{con} = 2 \cdot x_{N_2}^{con} \left[\frac{\text{kmol N}}{\text{kmol con.}}\right] \tag{28}$$

in which:

M_{H_2}, M_{O_2}, M_{N_2} – molar weights of the components in [kg/kmol],

X_{air} – moisture mass content related to dry air,

β_{steam} – steam to dry air mole factor in the converter,

γ_{CO_2} – CO_2 to dry air mole factor in the converter,

$x_{CO_2}^{con}$, $x_{H_2O}^{con}$, $x_{O_2}^{con}$, $x_{N_2}^{con}$ – molar fractions of gasifying agent ingredients in [%mol].

The molar weight of the feedstock fuel is defined as:

$$M_{fuel} = \left(\frac{C}{M_C} + \frac{H}{M_{H_2}} + \frac{O}{M_{O_2}} + \frac{N}{M_{N_2}} + \frac{S}{M_S} + \frac{w_{fuel}}{M_{H_2O}} \right)^{-1} \left[\frac{\text{kg fuel}}{\text{kmol fuel}}\right] . \tag{29}$$

The molar weight of the converter is determined by:

$$M_{con} = x_{CO_2}^{con} \cdot M_{CO_2} + x_{H_2O}^{con} \cdot M_{H_2O} + x_{O_2}^{con} \cdot M_{O_2} + x_{N_2}^{con} \cdot M_{N_2} \left[\frac{\text{kg con.}}{\text{kmol con.}}\right] \tag{30}$$

3.4. Deringer-Gumz equilibrium method with modification for propane

Deringer with Gumz modification equilibrium method for syngas calculation during gasification of sewage sludge is elaborated. Source of this method is from Kozaczka [14], where over a dozen of equilibrium methods were elaborated. The number of formulas for this model is much shortened in comparison to Kozaczka reference [14] or Gumz reference [68], due to the fact that the code in Microsoft Visual Basic was developed for iterative calculations, instead of manual calculations. Modified model is presented in authors previous work [3]. The method is based on the balance equation of gas components from gasification which follows the Dalton law:

$$x_{CO} + x_{CO_2} + x_{H_2} + x_{H_2O} + x_{CH_4} + x_{N_2} + x_{C_3H_8} + x_{SO_2} = 1 \tag{31}$$

Pseudocode scheme is presented in Fig. 3. Generally, the model focuses on iterative estimation of H_2 to CO mole fraction a ratio:

$$a = \frac{x_{H_2}}{x_{CO}} \tag{32}$$

Letters of b, c, d represent other ratios which needs to be calculated, respectively:

$$b = a^2 \cdot K_{(1)} \cdot K_{(3)} , \tag{33}$$

$$c = a \cdot K_{(4)} , \tag{34}$$

$$d = a^4 \cdot K_{(5)} \cdot K_{(1)}^2 \cdot p. \tag{35}$$

However, ratio d is a new modification to the original model of Deringer with Gumz modification and is related to propane formation.

For simplification of sulphur calculation in the model, reduced balances of particular elements mole concentrations including sulphur elements are introduced. Sulphur is treated as an inert in this model, thus it is being added to nitrogen mole concentration and treated as one $(NS)_{con}$ or $(NS)_{fuel}$ quantity:

$$(OS)_{con} = (O)_{con} - 2 \cdot (S)_{con} \left[\frac{\text{kmol}}{\text{kmol con.}}\right] \tag{36}$$

$$(NS)_{con} = (N)_{con} + (S)_{con} \left[\frac{\text{kmol}}{\text{kmol con.}}\right] \tag{37}$$

$$(OS)_{fuel} = (O)_{fuel} - 2 \cdot (S)_{fuel} \left[\frac{\text{kmol}}{\text{kmol fuel}}\right] \tag{38}$$

$$(NS)_{fuel} = (N)_{fuel} + (S)_{fuel} \left[\frac{\text{kmol}}{\text{kmol fuel}}\right] \tag{39}$$

Relations connected with k_1, k_2, k_3, k_4 are based on elements mole concentrations and their reduced balances, respectively:

$$k_1 = \frac{1}{2} \frac{(OS)_{con} \cdot (NS)_{fuel} - (OS)_{fuel} \cdot (NS)_{con}}{(C)_{fuel} \cdot (OS)_{con} - (C)_{con} \cdot (OS)_{fuel}} \tag{40}$$

$$k_2 = \frac{1}{2} \frac{(C)_{fuel} \cdot (NS)_{con} - (C)_{con} \cdot (NS)_{fuel}}{(C)_{fuel} \cdot (OS)_{con} - (C)_{con} \cdot (OS)_{fuel}} \tag{41}$$

$$k_3 = \frac{(C)_{con} \cdot (H)_{fuel} - (C)_{fuel} \cdot (H)_{con}}{(C)_{con} \cdot (OS)_{fuel} - (C)_{fuel} \cdot (OS)_{con}} \tag{42}$$

$$k_4 = \frac{(OS)_{fuel} \cdot (H)_{con} - (OS)_{con} \cdot (H)_{fuel}}{(C)_{con} \cdot (OS)_{fuel} - (C)_{fuel} \cdot (OS)_{con}} \tag{43}$$

The quite important step in sewage sludge gasification pseudocode is evaluation of A_1, B_1, C_1, A_2, B_2, C_2 equations, where C_1, C_2 are new to the original model related to the inclusion of propane formation:

$$A_1 = 1 + a + k_1 + k_2 \tag{44}$$

$$B_1 = 1 + b + c + (1 + b) \cdot k_1 + (2 + c) \cdot k_2 \tag{45}$$

$$C_1 = d + 3 \cdot k_1 \cdot d \tag{46}$$

$$A_2 = k_3 + k_4 - 2 \cdot a \tag{47}$$

$$B_2 = (2 + c) \cdot k_3 + (1 + b) \cdot k_4 - 4 \cdot b - 2 \cdot c \tag{48}$$

$$C_2 = 3 \cdot k_4 \cdot d - 8 \cdot d \tag{49}$$

Determination of CO and CO_2 molar fractions of produced gas from sewage sludge gasification are based on Dalton law, but the formulas are new in the literature with confirmation in previous article of authors. These equations are modified in comparison to Deringer model due to new steps being added which are related to propane formation.

The CO molar fraction is defined as:

$$x_{CO} = \frac{1 - B_1 \cdot x_{CO_2} - C_1 \cdot x_{CO_2}^2}{A_1} \ [\%\text{mol}] \tag{50}$$

The CO_2 molar fraction is determined from:

$$x_{CO_2} = \frac{(A_2 - C_1) \cdot \left(B_1 - \frac{A_1 \cdot B_2}{A_2} - \sqrt{\left(B_1 - \frac{A_1 \cdot B_2}{A_2} \right)^2 + 4 \cdot \left(C_1 - \frac{A_1 \cdot C_2}{A_2} \right)} \right)}{2 \cdot \frac{A_1 \cdot C_2}{A_2} - C_2} \ [\%\text{mol}] \tag{51}$$

Calculating iteratively criterial parameter $\kappa_{(1)}$ derived from iterations of a ratio, which must be almost equal to the target equilibrium constant $K_{(1)}$

$$\kappa_{(1)} \rightarrow K_{(1)} = \frac{x_{CO}^2}{x_{CO_2}} p \tag{52}$$

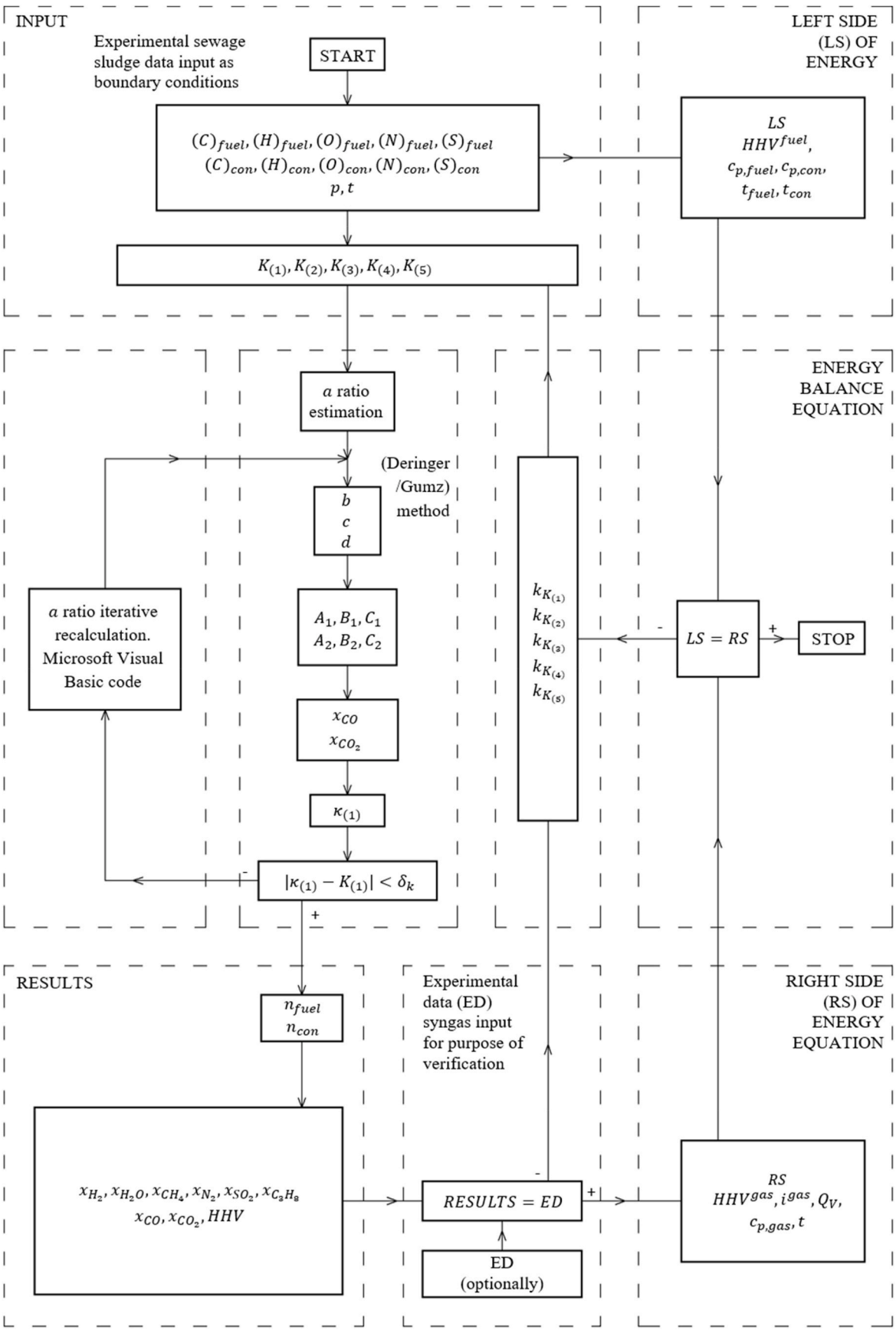

Fig. 3. Pseudocode implemented for gasifier.

Therefore, parameter $\kappa_{(1)}$ can be defined by Eqs. (50) and (51), and then it is iteratively determined based on the equilibrium constant of Boudouard reaction for the entire gasifier:

$$|\kappa_{(1)} - K_{(1)}| < \delta_k \tag{53}$$

After completing iterations where an assumed value of permissible error $\delta_k = 0.0001$ is met, the iterations are finished and results can be read.

In addition to CO and CO_2, the gasification process produces other components whose molar fractions have been determined as follows:

$$x_{H_2} = a \cdot x_{CO}\ [\%\text{mol}] \tag{54}$$

$$x_{CH_4} = b \cdot x_{CO_2}[\%\text{mol}] \tag{55}$$

$$x_{C_3H_8} = d \cdot x_{CO_2}^2[\%\text{mol}] \tag{56}$$

$$x_{H_2O} = c \cdot x_{CO_2}[\%\text{mol}] \tag{57}$$

New to the model is simple SO_2 mole fraction calculation, which is treated as an inert. SO_2 mole fraction calculation also affects N_2 mole fraction calculation due to the sulphur element being treated as sum with the nitrogen element in the earlier steps of the model:

$$x_{SO_2} = n_{fuel} \cdot (S)_{fuel} + n_{con} \cdot (S)_{con}[\%\text{mol}] \tag{58}$$

$$x_{N_2} = (k_1 + k_2) \cdot x_{CO} + ((1+b) \cdot k_1 + (2+c) \cdot k_2) \cdot x_{CO_2} + 3 \cdot d \cdot k_1 \cdot x_{CO_2}^2 - \frac{x_{SO_2}}{2}\ [\%\text{mol}] \tag{59}$$

where the mole amount of feedstock fuel per 1 kmole of produced gas is defined as:

$$n_{fuel} = \frac{(C)_{con} - (OS)_{con}}{(C)_{con} \cdot (OS)_{fuel} - (CS)_{fuel} \cdot (OS)_{con}} \cdot x_{CO} + \frac{(2+c) \cdot (C)_{con} - (1+b) \cdot (OS)_{con}}{(C)_{con} \cdot (OS)_{fuel} - (C)_{fuel} \cdot (OS)_{con}} \cdot x_{CO_2} - \frac{3 \cdot d \cdot (OS)_{con}}{(C)_{con} \cdot (OS)_{fuel} - (C)_{fuel} \cdot (OS)_{con}} \cdot x_{CO_2}^2 \left[\frac{\text{kmol fuel}}{\text{kmol gas}}\right] \tag{60}$$

And the mole amount of converter per 1 kmole of produced gas is determined by:

$$n_{con} = \frac{(OS)_{fuel} - (C)_{fuel}}{(C)_{con} \cdot (OS)_{fuel} - (C)_{fuel} \cdot (OS)_{con}} \cdot x_{CO} + \frac{\left(1+b\right) \cdot \left(OS_{)} - \left(2+c\right) \cdot (C)_{fuel}}{(C)_{con} \cdot (OS)_{fuel} - (C)_{fuel} \cdot (OS)_{con}} \cdot x_{CO_2} + \frac{3 \cdot d \cdot (OS)_{fuel}}{(C)_{con} \cdot (OS)_{fuel} - (C)_{fuel} \cdot (OS)_{con}} \cdot x_{CO_2}^2 \left[\frac{\text{kmol con.}}{\text{kmol gas}}\right] \tag{61}$$

3.5. Energy balance of gasifier

Due to the fact that Deringer method with Gumz modification does not include the inlet temperature of the converter and the inlet temperature of the feedstock, the model was extended to the energy balance equation, which is shown in the pseudocode. Predictions for the value of temperature T are based on the energy balance for the entire gasifier with respect to 1 kmole of gas, as follows:

$$n_{fuel} \cdot HHV^{fuel} + T \cdot \left(n_{fuel} \cdot c_p^{fuel} + n_{con} \cdot c_p^{con}\right) = HHV^{gas} + i^{gas} + Q_V \tag{62}$$

where:

n_{fuel} – feedstock fuel amount in [kmol fuel/kmol gas],
n_{con} – gasifying agent amount in [kmol con/kmol gas],
i^{gas} – molar specific enthalpy of gas in [kJ/kmol gas],
c_p^{fuel} – molar specific heat capacity of fuel in [kJ/kmol gas K],
c_p^{con} – molar specific heat capacity of gasifying agent in [kJ/kmol gas K],
HHV^{fuel} – molar specific higher heating value of fuel in [kJ/kmol gas],
HHV^{gas} – molar specific higher heating value of gas in [kJ/kmol gas],
Q_V – molar specific energy losses including ash in [kJ/kmol gas].

Thus, the pseudocode verifies the condition that the left-hand side of the equation equals the right-hand side according to what we can write the following:

$$LS = RS \tag{63}$$

and for this purpose, it should be further specified as a specific heat capacity of feedstock. In the model presented in this paper, the specific heat capacity was derived from two earlier publications, namely the work of Arlabosse et al. [69] and a book by Kozaczka [14]. The experimental curve developed by Arlabosse et al. [69] applies to the sewage sludge. Kozaczka's approximation [14], on the other hand, refers to inorganic substances using data on dry and ash-free substances. It is worth adding that the implementation and validation of both approaches will ensure mutual complementarity. The Arlabosse equation refers to the sewage sludge including ash. On the other hand, Kozaczka model [14], based on chemical elements without ash, determines the specific heat capacity for inorganic compounds. It should be noted that the selected sewage sludge sample for calibration purposes contains 56.94%wb organic fraction (58.1%db). Given the wide range of ash contents in the individual samples, the two ways of calculating the specific heat capacity discussed above should be used. Thus, we determine the specific heat capacity for the sewage sludge dry matter using the relationship [69]:

$$c_p^{fuel} = (1434 + 3.29 \cdot T) \cdot M_{dry\ fuel}\left[\frac{\text{kJ}}{\text{kmol gas} \cdot \text{K}}\right] \tag{64}$$

Although equation concerning dry ash free feedstock presented in Ref. [14] is as follows:

$$c_p^{fuel,af} = C \cdot c_{p,C(g)}(T) + H \cdot c_{p,H(g)}(T) + O \cdot c_{p,O(g)}(T) + N \cdot c_{p,Ng(g)}(T) + S \cdot c_{p,S(g)}(T)\ \left[\frac{\text{kJ}}{\text{kmol gas} \cdot \text{K}}\right] \tag{65}$$

The specific higher heating value of gas from gasification can be most accurately determined experimentally, however; it is possible to calculate using the mole fractions and higher heating values of individual combustible gases:

$$HHV^{gas} = \sum x_m \cdot HHV_m\left[\frac{\text{kJ}}{\text{kmol gas}}\right],\ m = CH_4, \ldots, CO_2 \tag{66}$$

while mole fractions x_m of gases $m = CH_4, \ldots, CO_2$ depends on the composition of resulted mixture. The universality of the model and the possibility of using fuel from gases of different compositions for combustion was tested in works [23].

3.6. Model of the gas scrubber

The primary purpose of the gas scrubber is to dry and purify the gases fed first to the compressor and then to the combustion chamber. Thus, in the resultant gas, the molar shares of the three components decrease to zero, namely: $x_{H_2O} = 0$, $x_{SO_2} = 0$, $x_{N_2} = 0$. Therefore, molar fractions of normalized components for dry, clean gas are as follows:

$$x_{CO}^{(d)} = \frac{x_{CO}}{1 - x_{H_2O} - x_{SO_2} - x_{N_2}}\ [\%\text{mol}] \tag{67}$$

$$x_{CO_2}^{(d)} = \frac{x_{CO_2}}{1 - x_{H_2O} - x_{SO_2} - x_{N_2}}\ [\%\text{mol}] \tag{68}$$

$$x_{H_2}^{(d)} = \frac{x_{H_2}}{1 - x_{H_2O} - x_{SO_2} - x_{N_2}} \ [\%\text{mol}] \tag{69}$$

$$x_{CH_4}^{(d)} = \frac{x_{CH_4}}{1 - x_{H_2O} - x_{SO_2} - x_{N_2}} \ [\%\text{mol}] \tag{70}$$

$$x_{C_3H_8}^{(d)} = \frac{x_{C_3H_8}}{1 - x_{H_2O} - x_{SO_2} - x_{N_2}} \ [\%\text{mol}] \tag{71}$$

Molar mass of dry and cleaned gas with normalized components:

$$M_{gas}^{(d)} = x_{CO}^{(d)} \cdot M_{CO} + x_{CO_2}^{(d)} \cdot M_{CO_2} + x_{H_2}^{(d)} \cdot M_{H_2} + x_{CH_4}^{(d)} \cdot M_{CH_4} + x_{C_3H_8}^{(d)} \cdot M_{C_3H_8} \tag{72}$$

where the unit includes information that is dry and clean gas $\left[\frac{\text{kg dry gas}}{\text{kmol dry gas}}\right]$.

Dry gas mass fractions are described as follows:

$$Y_{CO}^{(d)} = \frac{x_{CO}^{(d)} \cdot M_{CO}}{M_{gas}^{(d)}} \ [\%\text{mass}] \tag{73}$$

$$Y_{CO_2}^{(d)} = \frac{x_{CO_2}^{(d)} \cdot M_{CO_2}}{M_{gas}^{(d)}} \ [\%\text{mass}] \tag{74}$$

$$Y_{H_2}^{(d)} = \frac{x_{H_2}^{(d)} \cdot M_{H_2}}{M_{gas}^{(d)}} \ [\%\text{mass}] \tag{75}$$

$$Y_{CH_4}^{(d)} = \frac{x_{CH_4}^{(d)} \cdot M_{CH_4}}{M_{gas}^{(d)}} \ [\%\text{mass}] \tag{76}$$

$$Y_{C_3H_8}^{(d)} = \frac{x_{C_3H_8}^{(d)} \cdot M_{C_3H_8}}{M_{gas}^{(d)}} \ [\%\text{mass}] \tag{77}$$

3.7. Indicators defining quality of the resulting gas

However, sewage sludge can be used as a beneficial resource, it is important to develop a suitable technology of gasifiers or use an existing one to efficiently produce the gas. Gasification technology can be applied to convert the sewage sludge into useable gas what reduces the waste volume however it is necessary to introduce the indicators defining the quality of the resulting gas. Therefore, the mass of dry and cleaned gas derived from 1 kmole of total product gas is defined according to equation:

$$b_{\frac{gas}{gas}}^{(d)} = x_{CO} \cdot M_{CO} + x_{CO_2} \cdot M_{CO_2} + x_{H_2} \cdot M_{H_2} + x_{CH_4} \cdot M_{CH_4} + x_{C_3H_8} \cdot M_{C_3H_8} \left[\frac{\text{kg dry gas}}{\text{kmol gas}}\right] \tag{78}$$

It should be remembered that it is assumed $x_{H_2O} = 0$, $x_{SO_2} = 0$, $x_{N_2} = 0$. Another indicator is mass of dry and cleaned gas obtained from 1 kg of feedstock gasification, which formula including CO_2 from the gasifying agent is described according:

$$b_{\frac{gas}{fuel}}^{(d)} = \frac{b_{\frac{gas}{gas}}^{(d)}}{\left(x_{CO_2} + x_{CO} + x_{CH_4} + 3 \cdot x_{C_3H_8} - n_{con} \cdot x_{CO_2}^{con}\right)} \cdot \frac{C}{M_C} \left[\frac{\text{kg gas}}{\text{kg fuel}}\right] \tag{79}$$

or with using mole amount of feedstock fuel and molar weight is defined as follows:

$$b_{\frac{gas}{fuel}}^{(d)} = \frac{b_{\frac{gas}{gas}}^{(d)}}{M_{fuel} \cdot n_{fuel}} \left[\frac{\text{kg gas}}{\text{kg fuel}}\right] \tag{80}$$

Next, the mass of dry and cleaned gas obtained from 1 kg of gasifying agent can be determined by:

$$b_{\frac{gas}{con}}^{(d)} = \frac{b_{\frac{gas}{gas}}^{(d)}}{M_{con} \cdot n_{con}} \left[\frac{\text{kg gas}}{\text{kg con.}}\right] \tag{81}$$

Required mass of the converter per 1 kg of the fuel feedstock during gasification is calculated based on the following relationships:

$$b_{\frac{con}{fuel}} = \frac{M_{con} \cdot n_{con}}{M_{fuel} \cdot n_{fuel}} \left[\frac{\text{kg con.}}{\text{kg fuel}}\right] \tag{82}$$

3.8. Power output, efficiency, and emissions of nCO_2PP

Thermodynamic efficiency of the gasifying reactor of nCO_2PP, also labelled as cold gas efficiency, that is described by model in previous subsection, is determined by the following relation [70]:

$$\eta_R = \frac{LHV_{gas} \cdot \dot{m}_{2R}}{LHV_{fuel} \cdot \dot{m}_{SS} + I_{1R}} \ [\%] \tag{83}$$

where LHV_{gas} ; LHV_{fuel} are lower heating values for a created gas before gas scrubber (GS) calculated by ISO 6976:1995(E) and a sewage sludge as feedstock fuel calculated by standard method of Hysys, and I_{1R} is added enthalpy flow of gasifying agent from bleed turbine extraction, $\dot{m}_{2R}$ is mass flow of producer syngas before gas scrubber, and $\dot{m}_{SS}$ is sewage sludge mass flow to gasifying reactor.

But the hot gas efficiency refers to the dry and cleaned after gas scrubber that include additional energy from the cleaning process:

$$\eta_{R_H} = \frac{LHV_{DCgas} \cdot \dot{m}_{0^{fuel}} + I_{0^{fuel}}}{LHV_{fuel} \cdot \dot{m}_{SS} + I_{1R}} \ [\%] \tag{84}$$

where LHV_{DCgas} means lower heating value of obtained gas after the gas scrubber and $I_{0^{fuel}}$ is an additional enthalpy flow of hot gas.

The electrical power output of nCO_2PP can be defined based on output power of individual thermal cycle devices such as gas-steam turbine N_t, decreased due to power demand of such devices as compressors and water pumps. Therefore, the net electrical power of the entire system N_{net} can be calculated according to equation:

$$N_{net} = N_t - N_{cp} \ [\text{kW}] \tag{85}$$

where, $N_{cp}$is the electrical power demand for power plant own needs, respectively. The power for own needs N_{cp} is calculated by the following relationship:

$$N_{cp} = \dot{m}_{O_2} \eta_{mC} \left(h_{1^{O2}} - h_{0^{O2}}\right) + \dot{m}_{fuel} \eta_{mC} \left(h_{1^{fuel}} - h_{0^{fuel}}\right) + \dot{m}_{1^{CCU}} \eta_{mC} \left(h_{2^{CCU}} - h_{1^{CCU}}\right) + \dot{m}_{3^{CCU}} \eta_{mC} \left(h_{4^{CCU}} - h_{3^{CCU}}\right) + \eta_{m_{P-WCC}} N_{P-WCC} + \eta_{m_{P-SEC}} N_{P-SEC} \ [\text{kW}] \tag{86}$$

where $\dot{m}_{O_2}$, $\dot{m}_{1^{CCU}}$, $\dot{m}_{3^{CCU}}$ are the mass flow rate of oxygen from the ASU station and from gas scrubber, respectively, η_{mC} is the mechanical efficiency of the compressors, $\eta_{m_{P-WCC}}$, $\eta_{m_{P-SEC}}$ mechanical efficiency of pump driving water to WCC and SEC, respectively, including electrical motor and $h_{1^{O2}}$, $h_{0^{O2}}$, $h_{1^{fuel}}$, $h_{0^{fuel}}$, $h_{2^{CCU}}$, $h_{1^{CCU}}$, $h_{4^{CCU}}$, $h_{3^{CCU}}$ are the specific enthalpies of at individual points, N_{P-WCC}, N_{P-SEC} are energy flow required to drive water to the Wet Combustion Chamber and the Spray-Ejector Condenser. The power output of nCO_2PP turbines N_t is determined from the following relation:

$$N_t = \left[\dot{m}_2(h_2 - h_3) + \dot{m}_{3'}(h_{3'} - h_4)\right]\eta_{mGT} \ [\text{kW}] \tag{87}$$

where η_{mGT} is the mechanical efficiency of gas turbines including electrical generator, h_2, h_3, $h_{3'}$, h_4 are the specific enthalpy at individual points, and $\dot{m}_2$, $\dot{m}_{3'}$ is the mass flow rate in points 2 and point 3′ which is located after turbine bleed extraction to gasification reactor. Ultimately, the nCO_2PP efficiency can be determined as follows:

$$\eta_{net} = \frac{N_{net}}{LHV_{DCgas} \cdot \dot{m}_{0-fuel}} \ [\%] \tag{88}$$

A very important factor is the emissivity of the whole system, which is defined as follows [71]:

$$eCO_2 = R\frac{\dot{m}_{4-CO_2}}{N_{net}}3600\left[\frac{\mathrm{kgCO_2}}{\mathrm{MWh}}\right] \quad (89)$$

where $\dot{m}_{4-CO_2}$ represents mass flow rate of captured carbon dioxide, R is the factor only included for the power plant with the CO_2 capture that specifies fraction of energy source being treated as renewable by local law.

The calculation of emissivity requires special attention whether the system has CO_2 capture, if so the emission equals zero, but in the case of renewable energy source the value is negative. Some energy sources can be treated only in part as renewable according to the country's law, thus emissivity should be multiplied by factor that account this. In the emission analysis the relative emissivity of CO_2 is obtained by multiplying eCO_2 by η_{net}, as follows:

$$\eta_{net}\cdot e_{CO_2} = \frac{N_{net}}{LHV_{gas}\cdot\dot{m}_{0-fuel}}R\frac{\dot{m}_{4-CO_2}}{N_{net}}3600 = R\frac{\dot{m}_{4-CO_2}}{\dot{Q}_{CC}}3600\left[\frac{\mathrm{kgCO_2}}{\mathrm{MWh}}\right] \quad (90)$$

For the negative-emission power plants, avoided eCO_2 and analogically relative eCO_2 are the sum of emissivity without CO_2 capture ($R = 1$) and an absolute value of negative emissivity resulting from renewable energy ($|R| \leq 1$). For the zero-emission power plants avoided eCO_2 is only emissivity without CO_2 capture ($R = 1$).

The last parameter to consider in the context of the nCO_2PP cycle integrated with a gasification process is the determination of the cumulative efficiency. It reflects the electrical power transferred out of the system to the chemical energy flux delivered in the sludge, using the following formula:

$$\eta_{cum} = \frac{N_{net}}{LHV_{fuel}\cdot\dot{m}_{ss}} \sim \eta_{R_H}\cdot\eta_{net}\,[\%] \quad (91)$$

which is also depended on the hot gas efficiency η_{R_H} in relation to the net efficiency η_{net}.

Table 1
Assumptions for the thermodynamic cycle.

Parameter	Symbol	Unit	Value
Mass flow of the exhaust gas at the outlet from the combustion chamber WCC	$\dot{m}_2$	g/s	100
Air-fuel ratio in WCC	λ	–	1 (stoichiometric)
Temperature exhaust after WCC (before GT)	t_2	°C	1100
Initial fuel temperature	t_{fuel}	°C	50
Initial oxygen temperature	t_{O_2}	°C	15
Pressure of turbine bleed extraction/ gasification/converting agent	p_{O-R}, p_{2-R}	bar	0.7–1.6
Syngas fuel pressure before C_{fuel} compressor	p_{0-fuel}	bar	0.7–1.6
Oxygen pressure before C_{O2} compressor	p_{0-O_2}	bar	1
Fuel to WCC pressure loss factor	δ_{fuel}	–	0.05
Oxygen to WCC pressure loss factor	δ_{O_2}	–	0.05
Oxygen purity		%	99.9
Exhaust vapour quality after HE1	x_5	–	0.9999
Volumetric entrainment ratio in SEC	X	–	6
Motive fluid water pressure to SEC, before the nozzle	p_{1-SEC}	bar	6
steam quality in the SEC mixing chamber (fully condensed)	$x_{SEC-MC,o}$	–	~0
HE2 low temperature source		°C	15
HE2 mass flow of low temperature source		g/s	5000
CO_2 pressure after compressor C_{CCU1}	p_{2-CCU}	bar	25
CO_2 pressure after compressor C_{CCU2}	p_{4-CCU}	bar	80
H_2O temperature after HE4	t_{2-H_2O}	°C	110
CO_2 temperature after HE3	t_{3-CCU}	°C	115
Water vapour from Separator in 1^{CCU} mixed with CO_2 vapour		%	100% humid
Sewage sludge treated as renewable energy source by Polish law [72]	R	–	−0.9

Table 2
Assumed internal efficiency and mechanical efficiency, omitting the efficiency of the generator.

Internal efficiency:	Symbol	Unit	Value
Turbine GT	η_{iGT}	–	0.89
Turbine GT^{bap}	$\eta_{iGT-bap}$	–	0.89
Fuel compressor C_{fuel}	$\eta_{iC-fuel}$	–	0.87
Oxygen compressor C_{O2}	η_{iC-O2}	–	0.87
Water pump P_{H2O}	η_{iP-H2O}	–	0.8
Water pump P_{SEC}	η_{iP-SEC}	–	0.8
CO_2 compressor $C_{CO2\text{-}1}$	η_{iC-CO_2-1}	–	0.87
CO_2 compressor $C_{CO2\text{-}2}$	η_{iC-CO_2-2}	–	0.87
Mechanical efficiency for all devices	η_m	–	0.99

3.9. Assumptions to be made for the calculations and how to transfer information between calculation codes

The analysis was carried out for different values of pressure in bleed, ranging from 0.7 bar to 1.6 bar. The assumed parameters of the analysed cycle are contained in Table 1. Additionally, the assumed efficiencies for the devices are gathered in Table 2. There are presented also additional assumptions for nCO_2PP due to SEC and CCU addition. Vapour quality of the exhaust after HE1 is set as the assumption to use majority of regenerated heat instead of temperature change assumption on water side – vapour quality is set in order to treat this approach as reference for the optimalisation (what is the purpose of nCO_2PP).

The calculations were conducted within AspenONE engineering software package, which consists of the Aspen Plus, Aspen Hysys with integration of in-house code in the spreadsheet macro, presented in Fig. 4. Both Aspen Plus and Hysys were connected simultaneously to Excel spreadsheet through Aspen Simulation Workbook. Main thermodynamic power plant was simulated using Aspen Plus, gasification was calculated in spreadsheet model with macro using bleed turbine parameters from Aspen Plus, and the energy balance was conducted in Aspen Hysys to obtain gasification temperature. For ease of completing the thermodynamic model Aspen Plus was chosen due to higher level of complexity of the model which was to maintain exhaust mass flow, exhaust temperature, oxy-combustion, and spray-ejector condenser motive fluid water injection through various optimization techniques. The reason to employ Hysys for energy balance calculation was that it calculates in "Active" mode (similarly to the gasification spreadsheet model) with the simulation being ran every time something is changed, so all the iterations are completed immediately, while Aspen Plus is run after "Run" button is pressed and iterations are completed only within one simulation without changing input parameters. Worth to mention is the fact that Aspen Hysys has easily available proper reactor models to employ reaction constants, while completion of such task in Aspen Plus would require much greater effort. Compression, expansion and other processes are modelled in accordance with the thermodynamic tables (REFPROP (that combines accurate methods IAWPS-95 steam tables, GERG2008 for flue gas, etc.), Peng-Robinson state equations only for gasification in Aspen Hysys).

4. Results and discussion

4.1. Results of validation

Calibration of the gasification model was done in a previous paper by the authors [3]. The whole model was based on the extension to the energy equation and the formation of propane, with the remainder incorporating models from Ref. [14], where the main computing framework was established using Deringer method with Gumz modification. The model results were adjusted to the experimental results for the temperature of 760 °C by tuning the equilibrium constants using an approximation approach. The tuned coefficients are presented in Table 3. Equilibrium constants Eqs. (11-15) including these tuned

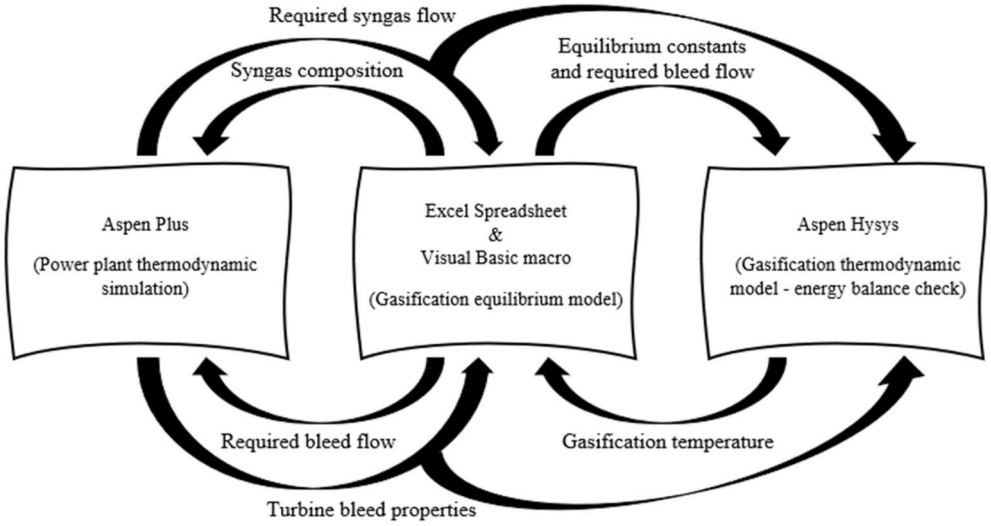

Fig. 4. Integration of in-house code for gasification with Aspen Plus, Aspen Hysys and Excel.

Table 3
Tuned coefficients for the equilibrium constants.

Equilibrium constant	Coefficient	Value
$K_{(1)}$	$k_{K_{(1)}}$	0.00224
$K_{(2)}$	$k_{K_{(2)}}$	–
$K_{(3)}$	$k_{K_{(3)}}$	19.3
$K_{(4)}$	$k_{K_{(4)}}$	1.031
$K_{(5)}$	$k_{K_{(5)}}$	$8.97 \bullet 10^{27}$

coefficients are crucial for the outcome of calculations. The results for higher temperatures are extended in the last article [3]. However, lower heating value and mass fraction of components of the calculated gas from steam gasification for 760 °C are compared in Table 4. For the lower heating value of resulted gas, the level of agreement was equal to 91%. In addition, a very important result obtained from the validation of the model at 760 °C is the general formula for the conversion of 1 kg of sewage sludge to gas from the gasification process:

$$C_{22.7}H_{64.8}O_{17.3}N_{3.1}S_{0.1}Ash_X(H_2O)_{1.1} + 1\ H_2O \xrightarrow{760^0C} 0.29\ CO + 0.99\ CO_2 + 2.09\ H_2 + 0.15N_2 + 0.01\ SO_2 + 0.14\ C_3H_8 + 0.57\ CH_4 + 6.1\ H_2O + XAsh \quad (92)$$

It should be noted that the gas composition shown in Table 4 is already after purification and drying, and the agreement of the model with experiment is at a very high level, and in the case of CO_2 it agrees in 100%. The differences obtained between the mathematical model and the experiment are small and it can be concluded that the model was properly validated. Basing on these results and comparison with other works from the literature [73] it is possible to perform gasification calculations for higher temperatures and for a changed composition of the converter, which will be presented in detail in the next subsection. For comparison, three selected results of gasification using turbine bleed of this work are added that are based on this model extrapolation. Additionally, it should be mentioned that the presented model provides a relatively high degree of confidence in the correctness of the results, due to the comparison with the results of Schweitzer et al. [73].

The difference that comes to the front between the reactor boundary conditions from the previous work and the model presented in this one is the admixture of CO_2 in the converting gas. The present CO_2 admixture is due to the fact that oxidation reactions of CO, CH_4 and C_3H_8 take place in the wet combustion chamber, which produce CO_2. In effect, a mixture of steam and CO_2 flows through the turbine stages, where part of this mixture is bleed extracted and directed to gasifying reactor as converting gas.

4.2. Extended calculation of integration of gasification with thermodynamic cycle for negative CO_2 power plant

As mentioned earlier, the gas-steam turbine cycle is coupled to the gasification reactor, and this interdependence best reflects the effect of pressure and temperature of the gasifying medium on the parameters in the gasifying reactor. According to Figs. 1 and 2, it can be concluded that there are no devices leading to pressure change in the path between the vent and the reactor, so the pressure in the reactor is very close to that of the extraction. On the other hand, the relationship between the

Table 4
Model validation of gasification with experimentally obtained syngas according to previous paper [3] and selected results of model extrapolation for this work.

Component	Symbol	Unit	Validation	Experiment	Extrapolation (using bleed turbine)		
CO fraction	$Y_{CO}^{(d)}$	%mass	11.4	13.6	39.3	42.6	46.8
CO_2 fraction	$Y_{CO_2}^{(d)}$	%mass	61.1	61.1	49.3	45.5	40.5
CH_4 fraction	$Y_{CH_4}^{(d)}$	%mass	12.8	11.7	4.0	4.2	4.5
C_3H_8 fraction	$Y_{C_3H_8}^{(d)}$	%mass	8.8	8.3	0.6	0.9	1.4
H_2 fraction	$Y_{H_2}^{(d)}$	%mass	5.9	5.3	6.8	6.8	6.9
Lower Heating Value	LHV_{gas}	MJ/kg	18.7	17.0	14.3	14.9	15.8
Temperature of the process	t_{2-R}	°C	760	760	923	968	1030
Pressure of the process	p_{2-R}	bar	1	1	0.7 ($=p_{0-R}$)	1 ($=p_{0-R}$)	1.6 ($=p_{0-R}$)
Gasifying agent (converter)	–	–	H_2O	H_2O	$CO_2 + H_2O$	$CO_2 + H_2O$	$CO_2 + H_2O$

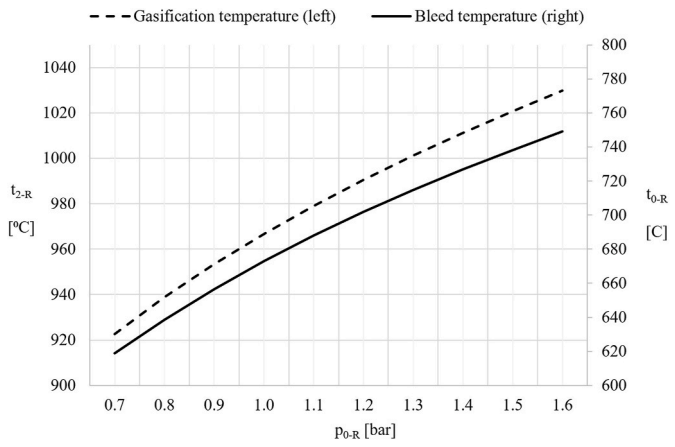

Fig. 5. Gasification and bleed temperature vs bleed pressure.

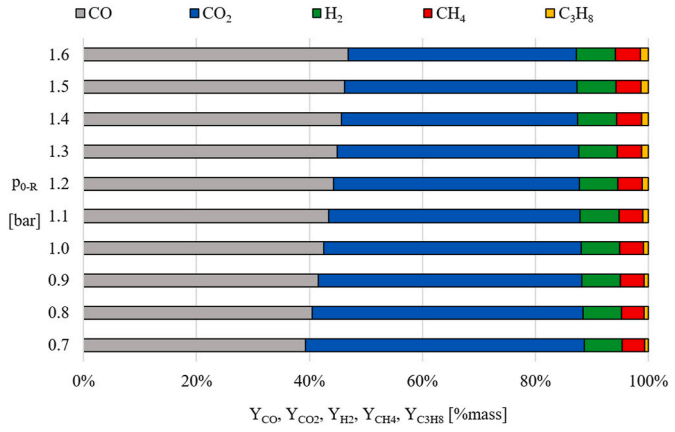

Fig. 6. Syngas mass fraction of CO, CO_2, H_2, CH_4, C_3H_8 vs bleed pressure. {color print}.

temperature of the extraction and the temperature in the reactor is not linear, and it is even apparent that the temperature rise in the gasifier flattens out with increasing pressure (Fig. 5).

Thus, as made evident by the equations for the equilibrium constants of chemical reactions (11–15), they are temperature dependent, and therefore temperature as one of the main stimuli (along with pressure and substrates) directly affects the composition of the resulting mixture. The mass fraction of individual components, namely: CO, CO_2, H_2, CH_4, C_3H_8 depending on the pressure and temperature in the bleed is shown in Fig. 6. Thus, at higher pressures and bleed temperatures, more CO (46.8% for 1.6 bar) than CO_2 (40.5% for 1.6 bar) is formed. The mass

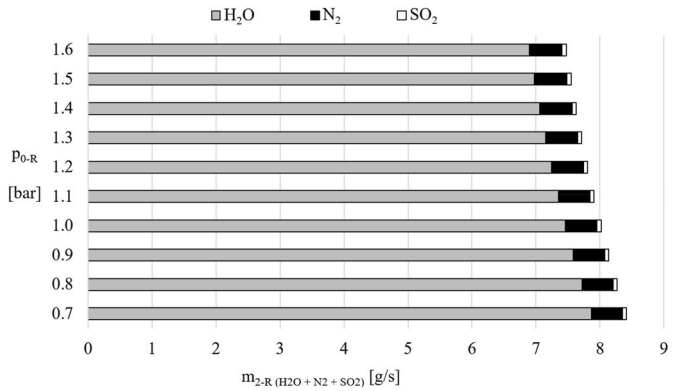

Fig. 7. Mass flow rate of H_2O, N2, SO_2 vs bleed pressure.

proportion of the other components remains fairly equal within 6.8–6.9% H_2 content. On the other hand, for lower bleed parameters the situation of CO and CO_2 mass shares is reversed and amounts to 39.3% for CO and 49.3 for CO_2 mass share at 0.7 bar. These values are related to the shift of chemical reaction equilibrium towards CO_2 and hydrocarbons for lower temperatures in the gasification reactor.

The difficulty in prediction of the fractions of individual components in the resultant gas can be analysed both in the pseudocode diagram and in the equations with reaction products, namely these complexities lie in the equilibrium constants of chemical reactions - Eqs. (5–10) and ratios between components - Eqs. (32-35). It should be mentioned that presented mass fractions were formed after the earlier separation of gases in the scrubber. The mass flow rate values of separated gases are shown in Fig. 7. The SO_2 content of the resulting gas remains at 0.062 g/s to 0.067 g/s for bleed pressures ranging from 0.7 bar to 1.6 bar. In addition to sulphur oxide, nitrogen also needs to be purified from the gasification gas, with values ranging from 0.49 to 0.51 g/s for the same extraction flows as before. The value of the water flow received is an order of magnitude higher than that of N_2 and two orders of magnitude higher than that of SO_2, but the resulting curve is of a different nature. This is because for a discharge pressure of 0.7 bar the highest water flow is received, namely more than 7.9 g/s, while for a discharge pressure of 1.6 bar 6.9 g/s is received.

Different fuel proportions affect the lower heating value of the dry and cleaned syngas as shown in Fig. 8. It increases with increasing pressure and temperature in the gasification reactor. And in turn, the increase in LHV is directly related to the improvement in conversion efficiency Eq. (84) of the gasification reactor where LHV of sewage sludge used to calculate this efficiency is calculated to be 17.12 MJ/kg in Hysys. Depending on the methods of treatment and stabilization processes applied in wastewater treatment facility, sewage sludge could have between 30 and 50% of ash content, thus having 50–70% of organic carbon [74]. Moreover, seasonal variations occur, and sewage sludge is generally heterogenous. This causes some variability of the heating value. Furthermore, different methods of determination of the heating value could also be the source of additional discrepancies. Bomb calorimetry is a standard method, where heating value is determined experimentally [75]. Werle and Dudziak [76] reported higher heating values (HHV) of 14.05 and 11.71 MJ/kg for sewage sludge after mechanical-biological and mechanical-biological-chemical treatment with phosphorus precipitation, respectively [76]. Pawlak-Kruczek et al. [77] reported HHV of 15.34 MJ/kg for their sewage sludge samples [77]. On the other hand, Aragón-Briceño et al. [78] used an empirical equation, formulated by Channiwala and Parikh [78,79], to estimate HHV based on CHNS composition of the sewage sludge digestate sample, and obtained HHV of 16.61 MJ/kg [78].

The mass flow rates describing the coupling between the cycle for

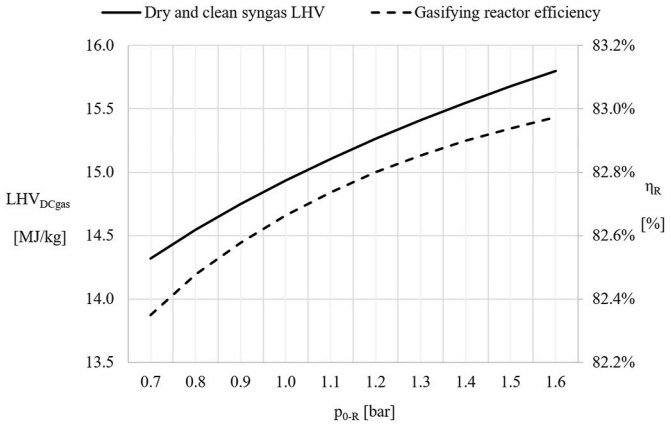

Fig. 8. Lower heating value and. conversion efficiency of the gasification reactor vs bleed pressure.

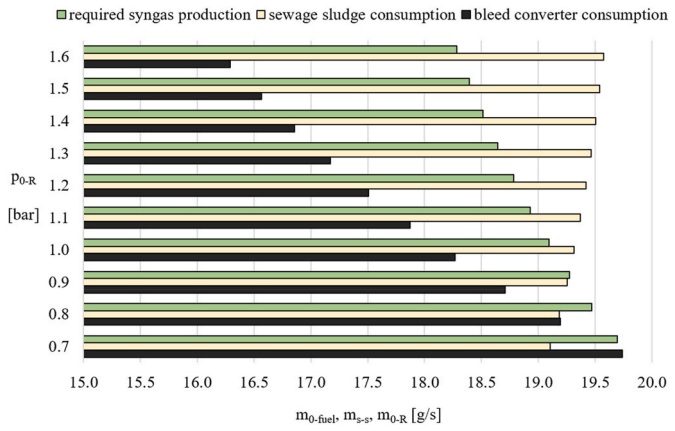

Fig. 9. Mass flow rate of required syngas production, sewage sludge and bleed converter consumption vs bleed pressure. {color print}.

negative CO_2 power plant and the gasification reactor are shown in Fig. 9. Thus, based on Fig. 9 showing the mass flow rates necessary for the operation and clustering of the system, it can be concluded that the fuel flow rate delivered to the combustion chamber does not change significantly. This is related to the fact that a constant temperature of 1100 °C is maintained in the combustion chamber during the simulations. As shown in Fig. 8, also the change of calorific value did not fluctuate significantly, so a stable level of fuel flow injected into the wet combustion chamber is justified (Fig. 9). On the other hand, the mass flux received for gasification varies much more depending on the bleed pressure. Thus, bleed converter consumption decreases by approx. 25%, namely from a value of 19.74 g/s at an extraction pressure of 0.7 bar to a value of 16.3 g/s at an extraction pressure of 1.6 bar. Only sewage sludge consumption increases as a result of the increase in pressure during the gasification process, as presented for $\dot{m}_{ss}$ in Fig. 9.

The wet combustion chamber is such an important facility that it is necessary to look in more detail at the issues of the effect of a change in bleed pressure on the mass flow rates of the various media supplied to it in order to maintain a temperature of 1100 °C and a working fluid flow of 100 g/s (Fig. 10). It should be noted that despite the decrease in fuel flow demand, the amount of oxygen injected increases as the bleed pressure increases. This is related to both the change in the components of the combustible mixture (Fig. 6) and the calorific value of the fuel (Fig. 8). The third medium introduced into the wet combustion chamber of the nCO_2PP cycle is water, whose mass flow rate increases slightly with increasing bleed pressure, namely from 61.7 to 62.7 g/s.

In principle, the resulting working fluid with a total mass flow of 100 g/s, after passing the high-pressure stages of the turbine (GT), enters the bleed, where the stream is divided into the part that flows through the

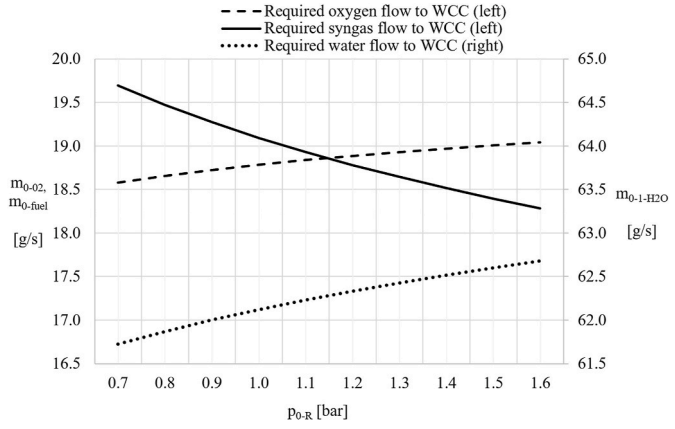

Fig. 10. Required oxygen, syngas and water flow to WCC vs bleed pressure.

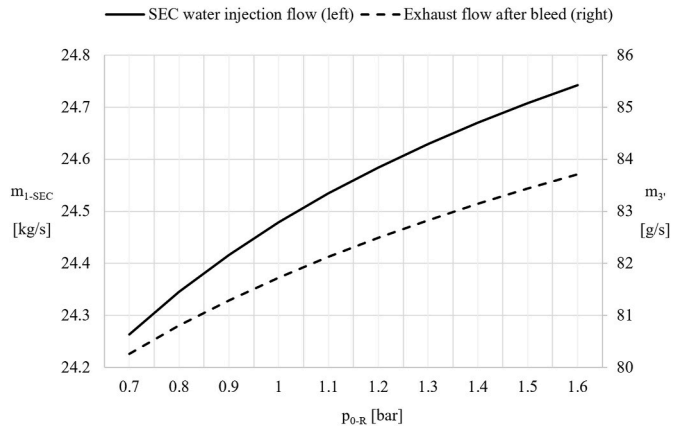

Fig. 11. Exhaust flow after bleed and SEC water injection flow vs bleed pressure.

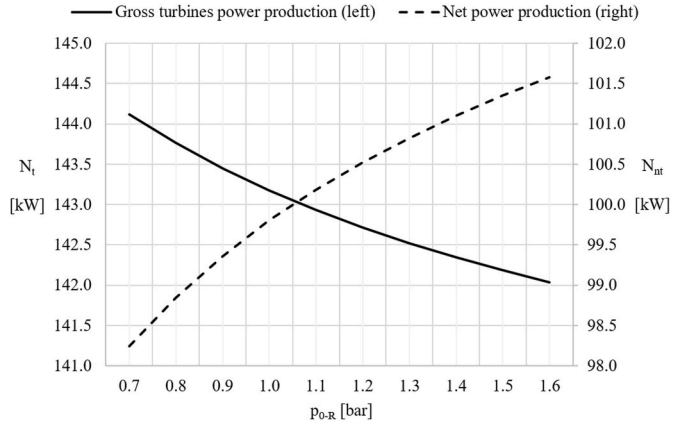

Fig. 12. Gross turbine power production and net power output vs bleed pressure.

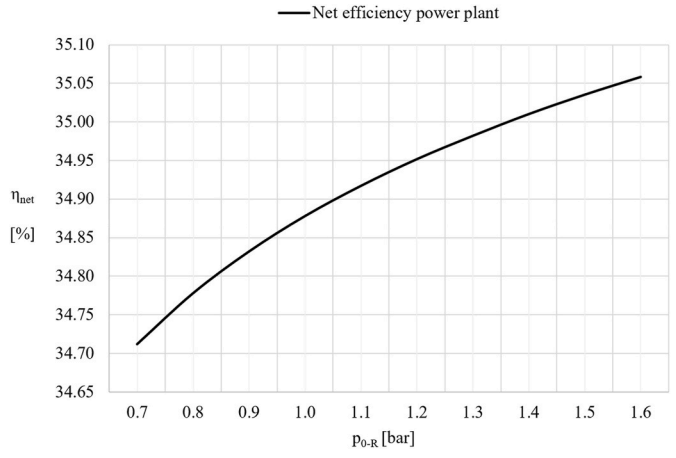

Fig. 13. Net efficiency power plant vs bleed pressure.

next turbine stages ($m_{3'}$) and the stream used as a gasifying medium (m_{0R}). Exhaust flow after bleed ($m_{3'}$) goes further into the SEC, where steam condensation and carbon dioxide separation take place due to water injection ($m_{1\text{-}SEC}$). The relationship between exhaust flow after bleed and SEC water injection flow vs bleed pressure is shown in Fig. 11. Both the flow entering SEC for steam condensation and CO_2 separation as well as the water driving this process increase with increasing bleed

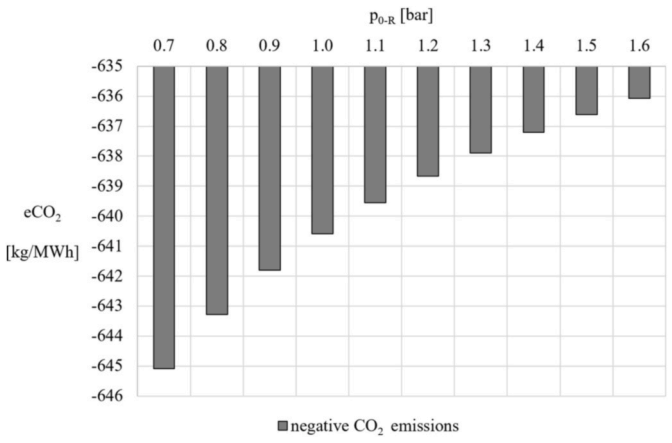

Fig. 14. Values of negative CO_2 emissions vs bleed pressure.

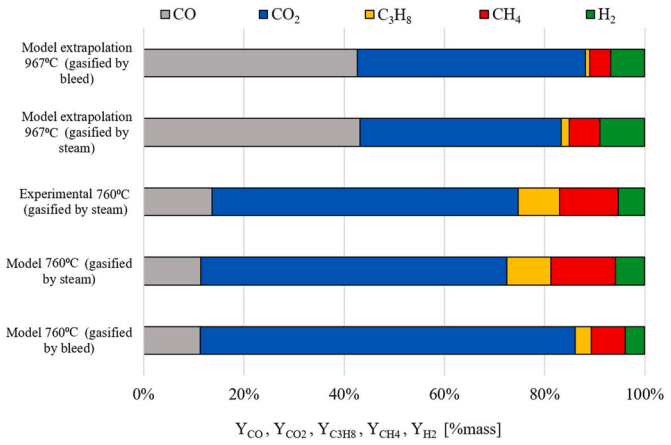

Fig. 16. Produced gas mass fractions vs gasification temperature and considered approach. {color print}.

pressure.

Quite significant results are shown in Figs. 12 and 13, where gross turbine power production, power output and net efficiency vs bleed pressure are presented, respectively. From this it can be concluded that as the pressure of the bleed increases, the net power and efficiency increases. On the other hand, the gross power decreases when the bleed pressure rises. However, in order to further investigate the performance of negative CO_2 emissions it is worth analysing Fig. 14, where production of carbon dioxide per 1 kWh of energy output is presented.

It is worth looking at Figs. 13 and 14 from the perspective of conventional power cycles. In CCGT units the emissivity of the plant decreases with increasing efficiency, i.e. in the older generation combined cycle featuring the efficiency of 41.2% the emissivity is 492 $kgCO_2$/MWh, while for the latest generation cycles at 60% efficiency the emissivity is around 330 $kgCO_2$/MWh [80].

In Figs. 13 and 14, the opposite trend appears, as with an increase in efficiency from 34.71 to 35.07%, the emissivity changes in the range from −646 $kgCO_2$/MWh to −736 $kgCO_2$/MWh. This relationship may be related to the fact that also the gross power of N_t turbines has a decreasing course vs. bleed pressure (Fig. 12). However, net efficiency and net power have an analogous course and in this context the emissivity is looked at in more detail in the further.

4.3. Comparison of converter changes at different temperatures

A comparison of the converter change at different temperatures is presented in two different figures, namely Figs. 15 and 16. A quite significant result is shown in Fig. 15, which presents a model generating a

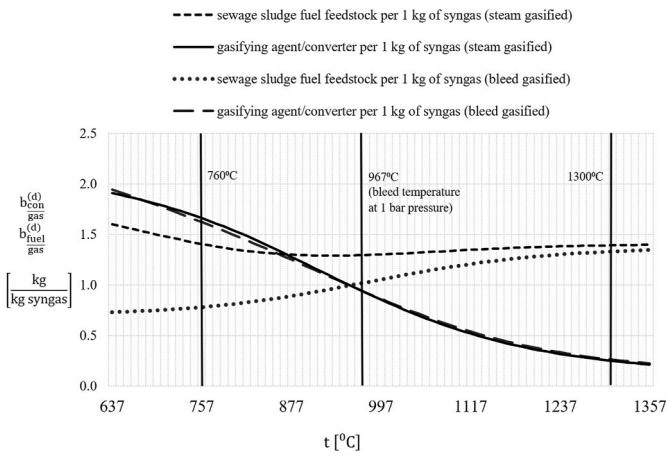

Fig. 15. Model generated required stacked amount of converter and sewage sludge feedstock to produce 1 kg of syngas vs gasification temperature.

required amount of converter and sewage sludge feedstock to produce 1 kg of syngas. From this it can be concluded that to produce 1 kg of syngas the amount of fuel feed is relatively constant at 1.5 kg for steam gasified in comparison to bleed gasified. The amount of converter per 1 kg produced gas decrease to reach a minimum value at 1357 °C in a quite similar way for both cases. Produced gas mass fractions vs gasification temperature is demonstrated in Fig. 16. There is some variation due to a shift in the chemical reaction equilibrium towards the component with the higher proportion in the converting gas.

4.4. Emissivity comparison of converter changes at different temperatures

Authors found that sewage sludge is treated in 90% as renewable energy source by Polish law [72], what was not accounted in their previous article [4]. In Fig. 14, power plant emissivity of CO_2 increasing from negative values with increasing bleed pressure is presented, while the net efficiency is also increasing (Fig. 13), what paradoxically suggests that lower efficiency power plant would be less harmful to the environment. Thus, a more practical qualitative definition for CO_2 negative emissivity should be sought. Table 5 presents comparison of emissivity of the nCO_2PP concept from authors previous article [4]. The results in table account for REFPROP calculation of the syngas mixture used in Ref. [3] as well as in this work (bleed extraction as gasification agent), but employs the Peng-Robinson equation of state for the work [3], as REFPROP doesn't include NO compound properties. Both calculations based on [3,4] syngas mixtures include aforesaid inclusion of a new sewage sludge emissivity factor [72]. The works [3,4] use two experimental syngases obtained from the same sewage sludge feedstock (same as in this work), syngas from work [4] has ammonia NH_3 component included and additional NO component in exhaust.

The values of obtained emissivities for the different cycle options and different fuel types (Table 5) indicate that the combined trend shown in Figs. 13 and 14 is repeated. To summarise the present relationships, it would be worthwhile to carry out a multi-criteria optimization that combines efficiency and emissivity and economic analysis that would provide interesting insight into the validity of such investment [81]. It should be mentioned that preliminary economic analyses have already been carried out for the cycle shown, and their results indicate that the investment is profitable, as it has a payback time of 4–6 years, depending on the assumptions made. The main economic returns from the nCO_2PP cycle are due to 3 revenue streams, namely: 1) from the disposal of sewage sludge from the wastewater treatment plant, 2) from CO_2 capture, emissions trading, and fee avoidance, 3) from the sale of electricity. Detailed information on the financial flows and the individual components of the economic analysis can be found in the authors' previous work [82].

Table 5
Negative CO_2 emission gas power plant comparison.

Parameter	Symbol	Unit	Experimental "mixture 2" syngas gasified at 760 °C by steam nCO_2PP	Experimental "mixture 1" syngas with NH_3 gasified by steam nCO_2PP	Modelled (this work) syngas gasified at 967 °C by 1 bar turbine bleed nCO_2PP
References	–	–	[3]	[4]	[this work]
Cumulative efficiency	η_{cum}	%	27.88	27.92	30.18
Net efficiency	η_{net}	%	39.48	39.40	34.88
CO_2 mass flow in exhaust	$\dot{m}_{4-CO2}$	g/s	23.15	22.68	19.73
Power for own needs	N_{cp}	kW	44.59	43.61	43.37
Turbine power output	N_t	kW	156.07	155.90	143.18
Chemical energy rate of combustion	$\dot{Q}_{CC}$	kW	282.38	284.86	286.1
Emission of carbon dioxide	eCO_2	$kgCO_2$/MWh	−672.76	−654.41	−640.58
Relative emissivity of carbon dioxide	$\eta_{net} \bullet eCO_2$	$kgCO_2$/MWh	−265.61	−258.03	−223.42
Avoided emission of carbon dioxide	Avoid eCO_2	$kgCO_2$/MWh	1420.27	1381.52	1352.34
Avoided relative emissivity of carbon dioxide	Avoid $\eta_{net} \bullet eCO_2$	$kgCO_2$/MWh	560.72	544.73	471.67

An additional quantity introduced in this work is cumulative efficiency η_{cum} calculated by Eq. (91), which accounts for the gasification process which was not covered by net efficiency η_{net} calculation Eq. (88) Eq. The cumulative efficiency is higher for this work concept of using turbine bleed as the gasifying converter, in comparison to lower cumulative efficiencies for the concepts without turbine bleed, which were based on syngas mixtures from Refs. [3,4], despite their increased net efficiencies in comparison to this work.

5. Conclusions

For the first time in the literature, the gasification model with the Deringer and Gumz modification was integrated into the gas turbine cycle by considering the mutual interaction of the bleed and the gasification reactor. In earlier work [3], C_3H_8 formation reactions were introduced into the original gasification model with the Deringer and Gumz modification and the overall mass balance was further verified at the energy balance level. The main novelty in the present model was the integration of the gasification with carbon dioxide and steam as the converter from the gas turbine bleed at varying temperature pressures of the gasification process. The challenge during calculation was to maintain constant exhaust mass flow of 100 g/s, while maintaining constant combustion temperature of 1100 °C in oxy-combustion manner, and all these while calculating gasification temperature through energy balance coupled with gasification model that requires specified gasifying agent (extracted turbine bleed from Aspen Plus simulation) mass flow to produce required syngas mass flow. It was possible by leveraging optimization techniques and automated iterations through Aspen and Excel programs. Even changes of the values across different bleed pressures prove the correctness of these simulations. The authors had not previously encountered a similar analysis in the literature, which allows for determination of the powers, efficiencies, and negative emissions of a power plant for the case of an integrated turbine and reactor system.

In general, as the bleed pressure increases, the efficiency of the nCO_2PP cycle integrated into the gasification process by bleeding the medium from the gas-steam turbine increases. It is important to say that cumulative efficiency of the nCO_2PP cycle with gasification unit increases thanks to the bleed extraction as gasifying agent despite lower net efficiency without gasification unit in comparison to nCO_2PP cycle with syngas [3,4] obtained in the concept presented in authors other work [4]. In general, cumulative efficiency will decrease after additional inclusion of air separation unit efficiency, but still efficiency optimization remains open through various other possibilities than presented in this work. From the work presented, it also becomes apparent that the gasification process is most influenced by the process temperature, followed by the converter composition and the last factor is the pressure prevailing in the gasification reactor.

CRediT author statement

Paweł Ziółkowski Conceptualization, Methodology, Software, Validation, Formal analysis, Investigation, Resources, Data curation, Writing—original draft preparation, Writing – review & editing, Visualization, Supervision, Project administration, Funding acquisition, **Kamil Stasiak** Conceptualization, Methodology, Software, Validation; Formal analysis, Investigation, Resources, Data curation, Writing—original draft preparation, Writing – review & editing, Visualization, **Milad Amiri** Formal analysis, Visualization, **Dariusz Mikielewicz** Conceptualization, Resources, Writing – review & editing, Supervision, Project administration, Funding acquisition. All authors have read and agreed to the published version of the manuscript.

Declaration of competing interest

The authors declare that they have no known competing financial interests or personal relationships that could have appeared to influence the work reported in this paper.

Data availability

All data are included within the article and attached supplements, or sourced from cited articles

Acknowledgements

The research leading to these results has received funding from the Norway Grants 2014–2021 via the National Center for Research and Development.

Article has been prepared within the frame of the project: "Negative CO_2 emission gas power plant" - NOR/POLNORCCS/NEGATIVE-CO2-PP/0009/2019–00 which is co-financed by programme "Applied research" under the Norwegian Financial Mechanisms 2014–2021 POLNOR CCS 2019 - Development of CO_2 capture solutions integrated in power and industry processes.

Appendix A. Supplementary data

Supplementary data to this article can be found online at https://doi.org/10.1016/j.energy.2022.125496.

References

[1] Essalhi N, Fguiri A, Marvillet C, Jeday MR. Design of helical coil condenser of small-capacity Water/Lithium Bromide absorption cooling machine. Int J Hydrogen Energy 2017;42:8888–97. https://doi.org/10.1016/j.ijhydene.2016.10.139.

[2] Vishwajeet, Pawlak-Kruczek H, Baranowski M, Czerep M, Chorążyczewski A, Krochmalny K, et al. Entrained flow plasma gasification of sewage sludge– proof-of-concept and fate of inorganics. Energies 2022;15:1–14. https://doi.org/10.3390/en15051948.

[3] Ziółkowski P, Badur J, Pawlak- Kruczek H, Stasiak K, Amiri M, Niedzwiecki L, et al. Mathematical modelling of gasification process of sewage sludge in reactor of negative CO2 emission power plant. Energy 2022;244. https://doi.org/10.1016/j.energy.2021.122601.

[4] Ziółkowski P, Madejski P, Amiri M, Kuś T, Stasiak K, Subramanian N, et al. Thermodynamic analysis of negative CO2 emission power plant using aspen plus, aspen Hysys, and ebsilon software. Energies 2021;14. https://doi.org/10.3390/en14196304.

[5] Amrollahi Z, Ertesvåg I S, Bolland O. Optimized process configurations of post-combustion CO2 capture for natural-gas-fired power plant—exergy analysis. Int J Greenh Gas Control 2011;5:1393–405. https://doi.org/10.1016/j.ijggc.2011.09.004.

[6] Mondino G, Grande CA, Blom R, Nord LO. Moving bed temperature swing adsorption for CO2 capture from a natural gas combined cycle power plant. Int J Greenh Gas Control 2019;85:58–70. https://doi.org/10.1016/J.IJGGC.2019.03.021.

[7] Amrollahi Z, Ystad PAM, Ertesvåg IS, Bolland O. Optimized process configurations of post-combustion CO2 capture for natural-gas-fired power plant – power plant efficiency analysis. Int J Greenh Gas Control 2012;8:1–11. https://doi.org/10.1016/J.IJGGC.2012.01.005.

[8] Piazzi S, Patuzzi F, Baratieri M. Energy and exergy analysis of different biomass gasification coupled to Fischer-Tropsch synthesis configurations. Energy 2022;249:123642. https://doi.org/10.1016/J.ENERGY.2022.123642.

[9] Shevyrev SA, Mazheiko NE, Yakutin SK, Strizhak PA. Investigation of characteristics of gas and coke residue for the regime of quasi- and non-stationary steam gasification of coal in a fluidized bed: Part 1. Energy 2022;251:123938. https://doi.org/10.1016/J.ENERGY.2022.123938.

[10] Ahlström JM, Walter V, Göransson L, Papadokonstantakis S. The role of biomass gasification in the future flexible power system – BECCS or CCU? Renew Energy 2022;190:596–605. https://doi.org/10.1016/J.RENENE.2022.03.100.

[11] Lund H, Werner S, Wiltshire R, Svendsen S, Thorsen JE, Hvelplund F, et al. 4th Generation District Heating (4GDH): integrating smart thermal grids into future sustainable energy systems. Energy 2014;68:1–11. https://doi.org/10.1016/J.ENERGY.2014.02.089.

[12] Sanaye S, Alizadeh P, Yazdani M. Thermo-economic analysis of syngas production from wet digested sewage sludge by gasification process. Renew Energy 2022;190:524–39. https://doi.org/10.1016/J.RENENE.2022.03.086.

[13] Bhaskar T, Balagurumurthy B, Singh R, Poddar MK. Thermochemical route for biohydrogen production. Biohydrogen 2013:285–316. https://doi.org/10.1016/B978-0-444-59555-3.00012-X.

[14] Kozaczka J. Procesy zgazowania : inżynierskie metody obliczeń. Kraków: Wydaw. AGH; 1994.

[15] Islam MW. Effect of different gasifying agents (steam, H2O2, oxygen, CO2, and air) on gasification parameters. Int J Hydrogen Energy 2020;45:31760–74. https://doi.org/10.1016/J.IJHYDENE.2020.09.002.

[16] Machin EB, Pedroso DT, Machín AB, Acosta DG, Silva dos Santos MI, Solferini de Carvalho F, et al. Biomass integrated gasification-gas turbine combined cycle (BIG/GTCC) implementation in the Brazilian sugarcane industry: economic and environmental appraisal. Renew Energy 2021;172:529–40. https://doi.org/10.1016/J.RENENE.2021.03.074.

[17] Castillo Santiago Y, Martínez González A, Venturini OJ, Sphaier LA, Ocampo Batlle EA. Energetic and environmental assessment of oil sludge use in a gasifier/gas microturbine system. Energy 2022;244:123103. https://doi.org/10.1016/J.ENERGY.2022.123103.

[18] Sikarwar VS, Zhao M, Clough P, Yao J, Zhong X, Memon MZ, et al. An overview of advances in biomass gasification. Energy Environ Sci 2016;9:2939–77. https://doi.org/10.1039/c6ee00935b.

[19] Ferreira S, Monteiro E, Brito P, Vilarinho C. A holistic review on biomass gasification modified equilibrium models. Energies 2019;12:1–31. https://doi.org/10.3390/en12010160.

[20] Basu P. Biomass gasification, pyrolysis and torrefaction: practical design and theory. Elsevier; 2013. https://doi.org/10.1016/C2011-0-07564-6.

[21] Żogała A. Equilibrium simulations of coal gasification – factors affecting syngas composition. J Sustain Min 2014;13:30–8. https://doi.org/10.7424/jsm140205.

[22] Costa M, La Villetta M, Massarotti N. Optimal tuning of a thermo-chemical equilibrium model for downdraft biomass gasifiers. Chem Eng Trans 2015;43:439–44. https://doi.org/10.3303/CET1543074.

[23] Cempa-Balewicz M, Jacek Łączny M, Smoliński A, Iwaszenko S. Equilibrium model of steam gasification of coal. J Sustain Min 2013;12:21–8. https://doi.org/10.7424/jsm130203.

[24] de Andrés JM, Vedrenne M, Brambilla M, Rodríguez E. Modeling and model performance evaluation of sewage sludge gasification in fluidized-bed gasifiers using Aspen Plus. J Air Waste Manag Assoc 2019;69:23–33. https://doi.org/10.1080/10962247.2018.1500404.

[25] Król D, Poskrobko S. High-methane gasification of fuels from waste – experimental identification. Energy 2016;116:592–600. https://doi.org/10.1016/J.ENERGY.2016.09.130.

[26] Sharma AK. Equilibrium and kinetic modeling of char reduction reactions in a downdraft biomass gasifier: a comparison. Sol Energy 2008;82:918–28. https://doi.org/10.1016/j.solener.2008.03.004.

[27] Jaworski TJ. Ocena metod obliczania parametrów zgazowania odpadów oraz ich eksperymentalna weryfikacja. Przem Chem 2015;94:1388–91. https://doi.org/10.15199/62.2015.8.28.

[28] Pala LPR, Wang Q, Kolb G, Hessel V. Steam gasification of biomass with subsequent syngas adjustment using shift reaction for syngas production: an Aspen Plus model. Renew Energy 2017;101:484–92. https://doi.org/10.1016/j.renene.2016.08.069.

[29] Ertesvåg IS, Kvamsdal HM, Bolland O. Exergy analysis of a gas-turbine combined-cycle power plant with precombustion CO2 capture. Energy 2005;30:5–39. https://doi.org/10.1016/J.ENERGY.2004.05.029.

[30] Adeyemi I, Janajreh I. Modeling of the entrained flow gasification: kinetics-based ASPEN Plus model. Renew Energy 2015;82:77–84. https://doi.org/10.1016/J.RENENE.2014.10.073.

[31] Rabea K, Michailos S, Akram M, Hughes KJ, Ingham D, Pourkashanian M. An improved kinetic modelling of woody biomass gasification in a downdraft reactor based on the pyrolysis gas evolution. Energy Convers Manag 2022;258:115495. https://doi.org/10.1016/J.ENCONMAN.2022.115495.

[32] Cerinski D, Ferreiro AI, Baleta J, Costa M, Zimbardi F, Cerone N, et al. Modelling the biomass updraft gasification process using the combination of a pyrolysis kinetic model and a thermodynamic equilibrium model. Energy Rep 2021;7:8051–61. https://doi.org/10.1016/J.EGYR.2021.05.079.

[33] Lewandowski MT, Ertesvåg IS. Analysis of the eddy dissipation concept formulation for MILD combustion modelling. Fuel 2018;224:687–700. https://doi.org/10.1016/J.FUEL.2018.03.110.

[34] Netzer C, Løvås T. Chemical model for thermal treatment of sewage sludge. Chem Eng 2022;6. https://doi.org/10.3390/chemengineering6010016.

[35] Gómez-Barea A, Leckner B. Modeling of biomass gasification in fluidized bed. Prog Energy Combust Sci 2010;36:444–509. https://doi.org/10.1016/j.pecs.2009.12.002.

[36] Mularski J, Pawlak-Kruczek H, Modlinski N. A review of recent studies of the CFD modelling of coal gasification in entrained flow gasifiers, covering devolatilization, gas-phase reactions, surface reactions, models and kinetics. Fuel 2020;271:117620. https://doi.org/10.1016/J.FUEL.2020.117620.

[37] Yepes Maya DM, Silva Lora EE, Andrade RV, Ratner A, Martínez Angel JD. Biomass gasification using mixtures of air, saturated steam, and oxygen in a two-stage downdraft gasifier. Assessment using a CFD modeling approach. Renew Energy 2021;177:1014–30. https://doi.org/10.1016/J.RENENE.2021.06.051.

[38] Rahma FN, Tamzysi C, Hidayat A, Adnan MA. Investigation of process parameters influence on municipal solid waste gasification with co2 capture via process simulation approach. Int J Renew Energy Dev 2021;10:1–10. https://doi.org/10.14710/ijred.2021.31982.

[39] Rupesh S, Muraleedharan C, Arun P. ASPEN plus modelling of air–steam gasification of biomass with sorbent enabled CO2 capture. Resour Technol 2016;2:94–103. https://doi.org/10.1016/J.REFFIT.2016.07.002.

[40] Stasiak K, Ziółkowski P, Mikielewicz D. Carbon dioxide recovery skid. Prog Petrochem Sci 2020;3:362–4. https://doi.org/10.31031/pps.2020.03.000570.

[41] Ziółkowski P, Zakrzewski W, Kaczmarczyk O, Badur J. Thermodynamic analysis of the double Brayton cycle with the use of oxy combustion and capture of CO2. Arch Therm 2013;34:23–38. https://doi.org/10.2478/aoter-2013-0008.

[42] Ziółkowski P. Porous structures in aspects of transpirating cooling of oxycombustion chamber walls. AIP Conf Proc 2019;2077. https://doi.org/10.1063/1.5091926.

[43] Bartela Ł, Skorek-Osikowska A, Kotowicz J. Economic analysis of a supercritical coal-fired CHP plant integrated with an absorption carbon capture installation. Energy 2014;64:513–23. https://doi.org/10.1016/j.energy.2013.11.048.

[44] Bolland O, Undrum H. A novel methodology for comparing CO2 capture options for natural gas-fired combined cycle plants. Adv Environ Res 2003;7:901–11. https://doi.org/10.1016/S1093-0191(02)00085-0.

[45] Kvamsdal HM, Jordal K, Bolland O. A quantitative comparison of gas turbine cycles with CO2 capture. Energy 2007;32:10–24. https://doi.org/10.1016/j.energy.2006.02.006.

[46] Anderson RE, MacAdam S, Viteri F, Davies DO, Downs JP, Paliszewski A. Adapting gas turbines to zero emission oxy-fuel power plants. Proc ASME Turbo Expo 2008;2:781–91. https://doi.org/10.1115/GT2008-51377.

[47] Anderson R, Hustad C, Skutley P, Hollis R. Oxy-fuel turbo machinery development for energy intensive industrial applications. Energy Proc 2014;63:511–23. https://doi.org/10.1016/j.egypro.2014.11.056.

[48] Anderson R, Viteri F, Hollis R, Hebbar M, Downs J, Davies D, et al. Application of existing turbomachinery for zero emissions Oxy-fuel power systems. Proc ASME Turbo Expo 2009;1:469–79. https://doi.org/10.1115/GT2009-59995.

[49] Jericha H, Sanz W, Woisetschläger J, Fesharaki M. CO2 - retention capapility of CH4/O2 - fired graz cycle. Cimac 1995:1–13.

[50] Jericha H, Göttlich E, Sanz W, Heitmeir F. Design optimization of the Graz cycle prototype plant. J Eng Gas Turbines Power 2004;126:733–40. https://doi.org/10.1115/1.1762910.

[51] Sanz W, Hustad C-WHJ. First generation GRAZ cycle power plant for near-term deployment. Proc ASME Turbo Expo 2011;2011. GT2011:GT2011-45135.

[52] Miller A, Lewandowski J, Badyda K, Kiryk S, Milewski J, Hama J, et al. Off-design analysis of the GRAZ cycle performance. Int Gas Turbine Congr 2003:1–6.

[53] Kotowicz J, Job M. Thermodynamic and economic analysis of a gas turbine combined cycle plant with oxy-combustion. Arch Therm 2013;34:215–33. https://doi.org/10.2478/aoter-2013-0039.
[54] Yantovsky E, Górski J, Shokotov M. Zero emissions power cycles. 2009. https://doi.org/10.1201/9781420087925.
[55] Yantovski EI, Zvagolsky KN, Gavrilenko VA. The COOPERATE - demo power cycle. Energy Convers Manag 1995;36:861–4. https://doi.org/10.1016/0196-8904(95)00139-5.
[56] Mathieu P, Nihart R. Sensitivity analysis of the MATIANT cycle. Energy Convers Manag 1999;40:1687–700. https://doi.org/10.1016/S0196-8904(99)00062-X.
[57] Fiaschi D, Manfrida G, Mathieu P, Tempesti D. Performance of an oxy-fuel combustion CO2 power cycle including blade cooling. Energy 2009;34:2240–7. https://doi.org/10.1016/j.energy.2008.12.013.
[58] Perrin N, Paufique C, Leclerc M. Latest performances and improvement perspective of Oxycombustion for carbon capture on coal power plants. Energy Proc 2014;63:524–31. https://doi.org/10.1016/j.egypro.2014.11.057.
[59] Staicovici MD. Further research zero CO2 emission power production: the "COOLENERG" process. Energy 2002;27:831–44. https://doi.org/10.1016/S0360-5442(02)00020-8.
[60] Chodkiewicz R, Porochnicki J, Kaczan B. Steam-gas condensing turbine system for power and heat generation. Proc ASME Turbo Expo 2001;2. https://doi.org/10.1115/2001-GT0097.
[61] Mikielewicz D, Wajs J, Ziółkowski P, Mikielewicz J. Utilisation of waste heat from the power plant by use of the ORC aided with bleed steam and extra source of heat. Energy 2016;97:11–9. https://doi.org/10.1016/j.energy.2015.12.106.
[62] Ziólkowski P, Mikielewicz D, Mikielewicz J. Increase of power and efficiency of the 900 MW supercritical power plant through incorporation of the ORC. Arch Therm 2013;34:51–71. https://doi.org/10.2478/aoter-2013-0029.
[63] Zheng S, Li C, Zeng Z. Thermo-economic analysis, working fluids selection, and cost projection of a precooler-integrated dual-stage combined cycle (PIDSCC) system utilizing cold exergy of liquefied natural gas. Energy 2022;238:121851. https://doi.org/10.1016/J.ENERGY.2021.121851.
[64] Yang D, Wang M, Yang R, Zheng Y, Pandzic H. Optimal dispatching of an energy system with integrated compressed air energy storage and demand response. Energy 2021;234:121232. https://doi.org/10.1016/J.ENERGY.2021.121232.
[65] Wu D, Bai J, Wei W, Chen L, Mei S. Optimal bidding and scheduling of AA-CAES based energy hub considering cascaded consumption of heat. Energy 2021;233:121133. https://doi.org/10.1016/J.ENERGY.2021.121133.
[66] Zhou Q, Du D, Lu C, He Q, Liu W. A review of thermal energy storage in compressed air energy storage system. Energy 2019;188:115993. https://doi.org/10.1016/J.ENERGY.2019.115993.
[67] Topolski J. PhD dissertation: "Diagnostyka spalania w układach gazowo - parowych.". In: Polish) - supervisor prof. Janusz Badur. IMP PAN Gdańsk (eng. IFFM PAS); 2002.
[68] Gumz W. Vergasung fester brennstoffe. 1952. https://doi.org/10.1007/978-3-662-13369-9.
[69] Arlabosse P, Chavez S, Prevot C. Drying of municipal sewage sludge: from a laboratory scale batch indirect dryer to the paddle dryer. Braz J Chem Eng 2005;22:227–32. https://doi.org/10.1590/S0104-66322005000200009.
[70] Pedroso DT, Machin EB, Proenza Pérez N, Braga LB, Silveira JL. Technical assessment of the biomass integrated gasification/gas turbine combined cycle (BIG/GTCC) incorporation in the sugarcane industry. Renew Energy 2017;114:464–79. https://doi.org/10.1016/j.renene.2017.07.038.
[71] Madejski P, Chmiel K, Subramanian N, Kus T. Methods and techniques for CO 2 capture : review of potential. Energies 2022;15:887.
[72] Ministerstwo Środowiska. Dziennik ustaw Rozporządzenie Ministra środowiska w sprawie warunków technicznych kwalifikowania części energii odzyskanej z termicznego przekształcania odpadów. 2016.
[73] Schweitzer D, Gredinger A, Schmid M, Waizmann G, Beirow M, Spörl R, et al. Steam gasification of wood pellets, sewage sludge and manure: gasification performance and concentration of impurities. Biomass Bioenergy 2018;111:308–19. https://doi.org/10.1016/j.biombioe.2017.02.002.
[74] Kacprzak M, Neczaj E, Fijałkowski K, Grobelak A, Grosser A, Worwag M, et al. Sewage sludge disposal strategies for sustainable development. Environ Res 2017;156:39–46. https://doi.org/10.1016/j.envres.2017.03.010.
[75] Pawlak-Kruczek H, Arora A, Gupta A, Saeed MA, Niedzwiecki L, Andrews G, et al. Biocoal - quality control and assurance. Biomass Bioenergy 2020;135:105509. https://doi.org/10.1016/J.BIOMBIOE.2020.105509.
[76] Werle S, Dudziak M. Gaseous fuels production from dried sewage sludge via air gasification. Waste Manag Res 2014;32:601–7. https://doi.org/10.1177/0734242X14536460.
[77] Pawlak-Kruczek H, Wnukowski M, Krochmalny K, Kowal M, Baranowski M, Zgóra J, et al. The staged thermal conversion of sewage sludge in the presence of oxygen. J Energy Resour Technol 2019;141:070701. https://doi.org/10.1115/1.4042822.
[78] Aragón-Briceño C, Ross ABB, Camargo-Valero MAA. Evaluation and comparison of product yields and bio-methane potential in sewage digestate following hydrothermal treatment. Appl Energy 2017;208:1357–69. https://doi.org/10.1016/j.apenergy.2017.09.019.
[79] Channiwala SA, Parikh PP. A unified correlation for estimating HHV of solid, liquid and gaseous fuels. Fuel 2002;81:1051–63. https://doi.org/10.1016/S0016-2361(01)00131-4.
[80] Kotowicz J, Brzęczek M, Job M. The thermodynamic and economic characteristics of the modern combined cycle power plant with gas turbine steam cooling. Energy 2018;164:359–76. https://doi.org/10.1016/J.ENERGY.2018.08.076.
[81] Ben Jabeur R, Fguiri A, Jeday MR, Chekir H, Fatnassi H, Marvillet C. Evaluation of the waste heat discharged from the Di-ammonium Phosphate production plant: a case study. J Mater Cycles Waste Manag 2018;20:1857–66. https://doi.org/10.1007/s10163-018-0727-4.
[82] Ziółkowski P, Pawlak-kruczek H, Madejski P, Bukowski P, Ochrymiuk T, Stasiak K, et al. Thermodynamic, ecological, and economic analysis of negative CO2 emission power plant using gasified sewage sludge. In: 2nd Int. Conf. Negat. CO2 Emiss., Göteborg; 2022.